VTT PUBLICATIONS 716

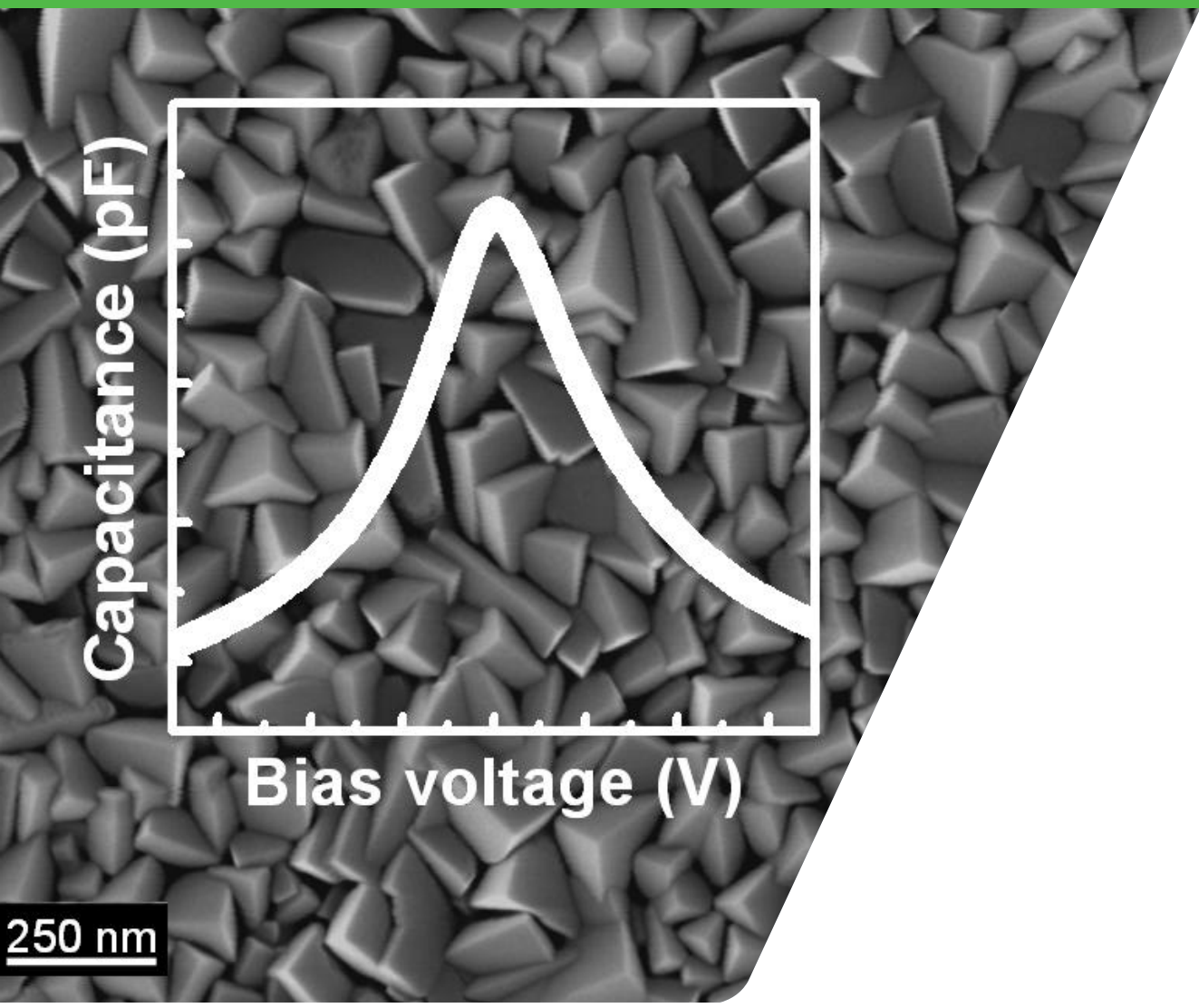

Tommi Riekkinen

Fabrication and characterization of ferro- and piezoelectric multilayer devices for high frequency applications

VTT PUBLICATIONS 716

Fabrication and characterization of ferro- and piezoelectric multilayer devices for high frequency applications

Tommi Riekkinen

Dissertation for the degree of Doctor of Science in Technology to be presented with due permission of the Faculty of Information and Natural Sciences, for public examination and debate in Auditorium E at Helsinki University of Technology (Otakaari 4, Espoo, Finland) on 2nd of November, 2009, at 12 noon.

ISBN 978-951-38-7356-1 (soft back ed.)
ISSN 1235-0621 (soft back ed.)

ISBN 978-951-38-7357-8 (URL: http://www.vtt.fi/publications/index.jsp)
ISSN 1455-0849 (URL: http://www.vtt.fi/publications/index.jsp)

JULKAISIJA – UTGIVARE – PUBLISHER

VTT, Vuorimiehentie 3, PL 1000, 02044 VTT
puh. vaihde 020 722 111, faksi 020 722 4374

VTT, Bergsmansvägen 3, PB 1000, 02044 VTT
tel. växel 020 722 111, fax 020 722 4374

VTT Technical Research Centre of Finland, Vuorimiehentie 3, P.O. Box 1000, FI-02044 VTT, Finland
phone internat. +358 20 722 111, fax + 358 20 722 4374

Technical editing Maini Manninen

Edita Prima Oy, Helsinki 2009

Tommi Riekkinen. Fabrication and characterization of ferro- and piezoelectric multilayer devices for high frequency applications [Ferro- ja pietsosähköisten monikerroskomponenttien valmistus ja karakterisointi suurtaajuussovelluksiin]. Espoo 2009. VTT Publications 716. 90 p. + app. 38 p.

Keywords Ferroelectric, Piezoelectric, $Ba_xSr_{1-x}TiO_3$, $Pb_xSr_{1-x}TiO_3$, AlN, Ta_2N, Ta_2O_5, Parallel-plate capacitor, Dielectric tuning, Dielectric loss, RF applications

Abstract

By means of thin film technology a reduction of size, cost, and power consumption of electronic circuits can be achieved. The required specifications are attained by proper design and combinations of innovative materials and manufacturing technologies. This thesis focuses on the development and fabrication of low-loss ceramic thin film devices for radio and microwave frequency applications. The materials, growth conditions, and physical properties of the films and device structures are discussed in detail. Moreover, special emphasis is placed on the integration of highly conductive low-loss electrode materials into parallel-plate structures.

The thin films were prepared by sequential magnetron sputtering from metallic and ceramic deposition targets. The devices under study include tunable ferroelectric barium strontium titanate and lead strontium titanate parallel-plate capacitors, and piezoelectric aluminum nitride thin film bulk acoustic wave resonators. Furthermore, tantalum pentoxide and tantalum nitride thin films were investigated for capacitor and resistor applications. As electrode material we used Au, Cu, Mo, and Pt. The use of highly conductive low-loss Cu electrodes was only possible after the development of a new layer transfer fabrication method for parallel-plate ceramic devices. This method, which was successfully used to fabricate tunable ferroelectric capacitors and AlN bulk acoustic wave resonators, allows for high-quality ceramic film growth on suitable substrate and seed layers and, most importantly, deposition of the bottom and top electrodes after high-temperature reactive sputtering of the ceramic material.

Optimization of the ceramic growth conditions and the integration of these functional materials into low-loss parallel-plate structures resulted in state-of-the-art device performance. Key achievements include, device quality factors of more than 100 up to GHz frequency in ferroelectric parallel-plate capacitors, the tailoring of ferroelectric film properties using substrate bias during magnetron sputtering, and very efficient electro-acoustic coupling in Mo/AlN/Mo bulk acoustic wave resonators.

Tommi Riekkinen. Fabrication and characterization of ferro- and piezoelectric multilayer devices for high frequency applications [Ferro- ja pietsosähköisten monikerroskomponenttien valmistus ja karakterisointi suurtaajuussovelluksiin]. Espoo 2009. VTT Publications 716. 90 p. + app. 38 p.

Avainsanat Ferroelectric, Piezoelectric, $Ba_xSr_{1-x}TiO_3$, $Pb_xSr_{1-x}TiO_3$, AlN, Ta_2N, Ta_2O_5, Parallel-plate capacitor, Dielectric tuning, Dielectric loss, RF applications

Tiivistelmä

Väitöstutkimuksessa perehdyttiin ohutkalvotekniikalla toteutettavien suurtaajuuspiirien rakennemateriaaleihin, niiden valmistustekniikkaan ja karakterisointiin. Ohutkalvotekniikan avulla voidaan toteuttaa pieniä, halpoja ja vähän energiaa vaativia komponentteja eri piiriratkaisuihin. Tämä vaatii uusien innovatiivisten materiaalien ja valmistusteknologioiden kehittämistä ja soveltamista. Tutkimuksessa kehitettiin pienihäviöisiä ohutkalvokomponentteja radio- ja mikroaaltotaajuussovelluksiin. Lisäksi kaikissa valmistetuissa rakenteissa käytettiin mahdollisimman hyvin johtavaa ja vähähäviöistä elektrodimateriaalia kriittisten suurtaajuushäviöiden vähentämiseksi.

Ohutkalvot valmistettiin sputteroimalla metalli- tai keraamikohtiosta. Työssä sovellettiin ferrosähköisiä bariumstrontium- ja lyijystrontiumtitanaatteja säädettäviin tasokondensaattorirakenteisiin. Tutkimuksessa kehitettiin myös valmistusprosessi pietsosähköisille alumiininitridiresonaattoreille suurtaajuussuodattimien rakenneosiksi. Lisäksi perehdyttiin ohutkalvokondensaattoreissa käytettävään tantaalipentoksidiin sekä ohutkalvovastuksissa sovellettavaan tantaalinitridiin. Elektrodimateriaaleina kaikissa rakenteissa käytettiin kultaa, kuparia, molybdeeniä tai platinaa. Väitöskirjassa esitetään lisäksi tapa valmistaa pienihäviöisiä ohutkalvorakenteita soveltamalla ns. kerrossiirtotekniikkaa. Tämä mahdollistaa minkä tahansa elektrodimateriaalin integroinnin rakenteisiin.

Tässä työssä valmistetut korkealaatuiset ohutkalvokomponentit ovat sovellettavissa suurtaajuusalueelle, ja ne edustavat alan tämän hetken uusinta tekniikkaa. Päätuloksina voidaan pitää ferrosähköisten komponenttien hyvyyslukua 100 yli GHz:n taajuusalueella, ferrosähköisten ohutkalvojen ominaisuuksien räätälöintiä substraattibiaksen avulla sekä korkeaa kytkentäkerrointa pietsosähköisissä resonaattoreissa.

Preface

The research for this thesis has been carried out in the Thin Film Components team at VTT Technical Research Centre of Finland. This work was supported by the Academy of Finland, Tekes – Finnish Funding Agency for Technology and Innovation, the European Community (the sixth Framework Programme) and VTT which are gratefully acknowledged. I am also thankful to the Jenny and Antti Wihuri Foundation and VTT for financial support to finalize the thesis.

I am most grateful to my supervisor, Professor Sebastiaan van Dijken, for his guidance and invaluable support during the work. I want to greatly thank my colleagues Dr. Jyrki Molarius, Mervi Hämäläinen, Dr. Arto Nurmela, Tuomas Pensala, Dr. Markku Ylilammi, Leif Grönberg, and Liisa Valkonen in the thin film components team for their help and cooperation. I wish to express my gratitude to many former and present co-workers at VTT: Dr. Joona Koponen, Päivi Majander, Dr. Jani Kivioja, Dr. Mika Prunnila, Dr. Jan Saijets, Dr. Tauno Vähä-Heikkilä, Unto Suominen, Hannu Hakojärvi, Jaakko Salonen, Kristiina Rutanen, Meeri Partanen, Satu Savolainen-Pulli, Leena Nurminen, Sami Vähänen, Dr. Kai Kolari, Ari Häärä, Hannu Luoto, Kimmo Henttinen and Dr. Tommi Suni, who contributed to the work. I would also like to express my special thanks to Dr. Tomi Mattila and Jorma Salmi for their collaboration, valuable discussions on the technical problems and everything else. Furthermore, I would like to thank Pasi Kostamo, Prof. Jorma Kivilahti, and Dr. Tomi Laurila at the Helsinki University of Technology for participating in the work. In addition, Dr. Ana Sánchez, Dr. Arne Lüker, Dr. Timo Sajavaara, and Leila Costelle are acknowledged for their contributions.

I want to thank my parents Leila and Heikki for their support. Finally, warmest thanks belong to my wife Päivi and to my adorable daughters Eva and Mona for their encouragement and patience throughout these years.

Contents

Appendices of this publication are not included in the PDF version. Please order the printed version to get the complete publication (http://www.vtt.fi/publications/index.jsp).

List of abbreviations and symbols

AC	Alternating current
AFM	Atomic force microscope
AlN	Aluminum nitride
BAW	Bulk acoustic wave
BCB	Benzo-cyclo-butene
BCC	Body-centered cubic
BST	Barium strontium titanate
BTO	Barium titanate
BZN	Bismuth zinc niobate
CMP	Chemical mechanical polishing
CVD	Chemical vapour deposition
CTE	Coefficient of thermal expansion
DC	Direct current
DRIE	Deep reactive ion etcher
FCC	Face-centered cubic
FOM	Figure of merit
FWHM	Full width at half maximum
HTS	High-temperature superconductor
IC	Integrated circuit
ICP	Inductively coupled plasma
MBE	Molecular beam epitaxy
MEMS	Micro-electro-mechanical systems
MIM	Metal-insulator-metal
MOCVD	Metalorganic chemical vapour deposition
PLD	Pulsed laser deposition
PPM	Parts per million
PST	Lead strontium titanate
PVD	Physical vapour deposition
PZT	Lead zirconate titanate
Q	Quality factor
RBS	Rutherford backscattering spectroscopy
RF	Radio frequency
RIE	Reactive ion etching
RMS	Root mean square

SAW	Surface acoustic wave
SEM	Scanning electron microscopy
SMR	Solidly mounted resonator
SOI	Silicon-on-insulator
STO	Strontium titanate
TCR	Temperature coefficient of resistance
TEM	Transmission electron microscopy
UHV	Ultra high vacuum
VCO	Voltage controlled oscillator
VNA	Vector network analyzer
VTT	Technical Research Centre of Finland
XRD	X-ray diffraction
XRR	X-ray reflectivity
ZnO	Zinc oxide

α	Decay constant
A	Area
C	Capacitance
Cw	Curie-Weiss constant
d_{die}	Thickness of dielectric
d_{ele}	Thickness of electrode
δ	Skin depth
E	Electric field, Young's modulus
ε_0	Permittivity of free space
ε_r	Relative dielectric constant
ϕ	Impedance phase
f	Frequency
f_p	Parallel resonance frequency
f_s	Series resonance frequency
K^2	Effective electro-acoustic coupling coefficient
l	Length
μ	Magnetic permeability
P_s	Spontaneous electric polarization
Q_{tot}	Total quality factor
Q_{die}	Dielectric quality factor
Q_{ele}	Electrode quality factor
ρ	Resistivity, Material density

R	Resistance
T	Temperature
$\tan\delta$	Loss tangent
T_c	Curie temperature
w	Width
ω	Angular frequency
X_L	Inductive reactance
Z	Acoustic impedance
Z_0	Line impedance
Z_{in}	Input impedance

List of publications

I Riekkinen, T., Mattila, T., Van Dijken, S., Lüker, A., Zhang, Q., Kirby, P. & Sánchez, A. Ferroelectric parallel-plate capacitors with copper electrodes for high-frequency applications. Applied Physics Letters, 2007. Vol. 91, 252902-1-3.

II Riekkinen, T., Molarius, J. & Ylilammi, M. Electrode metallization for high permittivity oxide RF thin film capacitors. Journal of the European Ceramic Society, 2007. Vol. 27, pp. 2983–2987.

III Riekkinen, T. & Molarius, J. Reactively sputtered tantalum pentoxide thin films for integrated capacitors. Microelectronic Engineering, 2003. Vol. 70, pp. 392–397.

IV Riekkinen, T., Molarius, J., Laurila, T., Nurmela, A., Suni, I. & Kivilahti J.K. Reactive sputter deposition and properties of Ta_xN thin films. Microelectronic Engineering, 2002. Vol. 64, pp. 289–297.

V Riekkinen, T., Nurmela, A., Molarius, J., Pensala, T., Kostamo, P., Ylilammi, M. & van Dijken, S. Influence of the seed layer on structural and electro-acoustic properties of sputter-deposited AlN resonators. Thin Solid Films, 2009, article in press.

VI Riekkinen, T., Saijets, J., Kostamo, P., & van Dijken, S. Influence of substrate bias on the structural and dielectric properties of magnetron-sputtered $Ba_xSr_{1-x}TiO_3$ thin films. arXiv:0909.1637v1 [cond-mat.mtrl-sci], 2009.

Author's contribution

The contribution of the author is described below.

Publication I: The author together with Tomi Mattila and Sebastiaan van Dijken was responsible for the research plan, electrical and structural characterization of the thin films, interpretation of the results and manuscript preparation. Arne Lüker prepared the ferroelectric thin film and the final devices were fabricated by the author. Ana Sánchez carried out the TEM analysis.

Publication II: The author was responsible for the research plan, performed the experimental work and interpretated the results. The author prepared the manuscript together with the co-authors.

Publication III: The author was responsible for the research plan, performed the experimental work and interpretated the results. Arto Nurmela carried out the RBS analysis. The author prepared the manuscript together with the co-author.

Publication IV: The author was responsible for the research plan and performed the experimental work. Arto Nurmela performed the RBS analysis. The interpretation of the results and manuscript preparation were carried out by the author together with the co-authors.

Publication V: The author together with the co-authors was responsible for the research plan, interpretation of the results and manuscript preparation. The author prepared the devices. The high frequency characterization and XRD measurements were carried out by Arto Nurmela and Pasi Kostamo, respectively.

Publication VI: The author together with the co-authors was responsible for the research plan, interpretation of the results and manuscript preparation. The author prepared the devices. The electrical characterization was performed by the author together with Jan Saijets. Timo Sajavaara performed the RBS analysis. XRD measurements were carried out by Pasi Kostamo.

1. Introduction

The requirement for mobile access to computing and communication services is ever-increasing. In response to this demand, a wide variety of portable gadgets is currently under development. These wireless devices utilize a number of radio frequency (RF) circuits. The primary criteria for electronic circuit components include small size, low power consumption (increase in operation time of hand-held devices) and low cost. Thin film technology enables the integration of components to form completely miniaturized circuits. The interesting features of this technology are the small component size and the ability to tailor material properties by changing the deposition conditions. Advancements of electronic circuits will be realized by the development and integration of functional materials and manufacturing solutions. The aim of this study is to develop and improve the fabrication technologies of thin films and thin film devices for RF and microwave applications. The thesis is divided into four research topics: ferroelectric, piezoelectric, other dielectric and resistive thin films, and their electrode metallurgy.

High frequency properties of thin film devices depend not only on the functional material itself but also on the electrodes. Firstly, as the bottom electrode serves as seed layer for subsequent ceramic film growth, it should provide a high degree of crystalline texture, limited surface roughness, and good thermal and chemical stability. Moreover, the quality factor of the devices is often dominated by electrode losses at microwave frequencies [1–7]. Hence, the integration of highly conducting low-loss electrode materials such as Ag, Au, Cu, and Mo is crucial to improve the device performance.

In mobile device applications the impedance of the antenna is not constant during regular use. An adaptive matching circuit is therefore needed to minimize the RF signal reflection losses between the antenna and the electronic circuit. Currently, tunable devices in the RF band are not in use. The potential solutions

include RF microelectromechanical system (MEMS), semiconductor based tunable capacitors and the use of ferroelectric materials [7–15] with a dielectric permittivity that can be controlled by an electric field. Besides the high dielectric tunability, ferroelectric materials exhibit many other desirable properties including relatively low dielectric loss in the paraelectric phase, fast polarization response, and high breakdown field. Barium strontium titanate (BST) is one of the most intensively studied materials. The dielectric properties of ferroelectric thin films depend on deposition method, deposition temperature, growth rate, process pressure, composition, lattice strain, and film thickness [9, 12, 14, 16–20]. Precise control of the complex fabrication process is essential to achieve the desired properties at high operation frequencies. The successful integration of these materials into parallel-plate capacitors with low-loss electrodes is of interest to various tunable device applications such as phase shifters and tunable switches, matching networks, filters, and resonators. However, the integration has been problematic and this has hampered large scale industrial applications. The main issues relate to the high deposition temperature (600–800 °C) and reactive atmosphere that are necessary requirements for the growth of high-quality crystalline ferroelectric thin films and this poses limitations on the selection of suitable electrode materials.

Other indispensible components for wireless systems are radio-frequency filters. Thin film capacitors and inductors can be used as a filter. However, the large size and low quality factor of the inductor limit the attractiveness of this solution for mobile device applications. Alternatively, piezoelectric material [21] can be used as a proxy for thin film inductors. This approach uses the resonance of a generated sound wave as a basis for the filtering of RF signals. Potential materials for the acoustic resonators are zinc oxide (ZnO) and aluminum nitride (AlN) [22–32]. At present, AlN is predominantly used as piezoelectric material in thin film bulk acoustic wave devices as it exhibits a good effective electro-acoustic coupling coefficient and it is very stable and compatible with micro-electronic IC-processing. To fulfill the device requirements in, for example, mobile phone applications, the AlN film must be of very high quality. Deposition of a perfectly oriented piezo-layer is difficult and therefore special care must be taken when considering the deposition process parameters, electrodes, and process chamber.

Completely miniaturized circuits for RF and microwave applications also require other passive RF components such as thin film isolation capacitors and thin film bias resistors. Tantalum-based materials are interesting alternatives for

these devices. Tantalum pentoxide (Ta_2O_5) exhibits a high dielectric constant and this can be used to reduce the capacitor size. Tantalum nitride (TaN) is chemically stable and its resistivity can be tailored by the deposition parameters. In addition, for good high-frequency properties, integration of these structures with low-loss electrodes is required.

1.1 Scope and contents of the thesis

This thesis focuses on the development and fabrication of low-loss thin film devices for RF and microwave applications. The potential materials for the devices are described as well as their growth characteristics and physical properties. The emphasis is placed on ferro- and piezoelectric thin films for tuning and resonator applications. Furthermore, thin film capacitors and resistors utilizing tantalum-based materials are presented. Integration of these thin film structures with highly conductive electrode materials is also demonstrated. The research has been carried out in the Thin Film Components team at VTT Technical Research Centre of Finland.

The thesis is divided into two parts: an overview of the scientific results and six journal publications. In the first part, Chapter 2 discusses the experimental methods that were utilized for the deposition and characterization of thin ceramic films and device structures. The high-frequency properties of electrodes such as the frequency dependence of the *Q*-value are described in Chapter 3. Here, special emphasis is placed on the stability of different bottom electrode materials during ceramic film growth. In Chapter 4 a new method that was developed during the course of this study, for integration of low-loss electrodes with high-quality ceramic films is introduced. This method is based on the transfer of a multilayer structure from an auxiliary substrate to a device substrate. The fabrication of parallel-plate devices using adhesive bonding, Au-Au bonding and direct wafer bonding are discussed.

The next three chapters of the thesis describe the materials, growth, and characterization of the various device structures. Chapter 5 deals with ferroelectric thin films. The fundamental properties of the ferroelectric films are shortly reviewed. The effect of process parameters, especially substrate bias, on the properties of magnetron sputtered BST thin films are described. In addition, the performance of low-loss Cu/BST/Cu parallel-plate devices, that are fabricated using the new layer transfer method, is reviewed. In Chapter 6 piezoelectric materials for signal filtering applications at GHz operating frequency are introduced. The

emphasis is on the optimization of Mo electrode on which the piezoelectric film is grown. The properties of AlN deposited onto these Mo electrodes are given. In addition, demonstration of AlN-based resonator utilizing the layer transfer is shown. Other passive devices such as thin film Ta_2O_5 capacitors and TaN resistors are discussed in Chapter 7. The process compatibility of the resistors and capacitors with Cu electrodes is also presented. Chapter 8 summarizes the work.

2. Experimental methods

This chapter introduces the deposition techniques that were used to grow the ceramic thin films and multilayer structures. Also, the most intensively used analytical methods for material and device characterization are described.

2.1 Thin film deposition

A number of different techniques can be used for the deposition of ceramic thin films. Among these are magnetron sputtering, pulsed-laser deposition (PLD), chemical vapor deposition (CVD) and molecular beam epitaxy (MBE). In addition, spin-coating of precursor solutions onto a substrate to produce thin films, the so-called sol-gel method, is commonly used. The ceramic thin films fabricated in this study were deposited using magnetron sputtering and sol-gel.

2.1.1 Sol-gel deposition

The sol-gel method was used to grow ferroelectric thin films [I]. In this method several spin coating/drying cycles of the precursion solution are conducted at room temperature (spin coating) and moderate temperatures (drying) to achieve the desired film thickness. The resulting film is then crystallized by annealing at elevated temperatures, generally > 600 °C for ferroelectric materials. The method is flexible and inexpensive, but disadvantages such as reproducibility and control over crystalline phases and film composition limit its large scale application potential.

2.1.2 Magnetron sputtering

Magnetron sputtering was utilized to fabricate several ceramic thin films and electrode structures [I–VI]. The advantages of magnetron sputtering include

precise control over film composition, thickness, and uniformity. The films were sputtered in a von Ardenne CS 730 S cluster tool. The tool consisted of three process chambers, a load lock, and a dealer chamber. One chamber was equipped with three magnetron guns and a hollow cathode sputter etcher. This chamber was dedicated to the growth of oxide films using RF magnetron sputtering. The second chamber consisted of four DC magnetron guns for metal film growth. The third chamber was exclusively used for AlN deposition via pulsed-DC magnetron sputtering in an ultra-clean environment. Because high temperature was required for proper film crystallization, custom made halogen lamp heaters were installed above the substrate holder. A substrate temperature of 750 °C was reached with these heaters.

The typical magnetron sputtering methods include DC sputtering, RF sputtering, and pulsed-DC sputtering. The sputtering system consists of a cathode (the target) and an anode (the chamber wall and substrate holder). The substrate holder can be floating, grounded, or biased. The simplest configuration for magnetron sputtering is the DC mode which is generally used for conducting metals. The highly conducting electrode metallizations used in our study were deposited using DC magnetron sputtering [I–VI]. The sputtering of insulating films with a DC power supply is limited by a charging effect on the target and the resulting reduction of sputtering rate. RF magnetron sputtering is therefore used for the deposition of insulating materials. In this case, a RF power supply equipped with impedance matching network is used to generate the sputtering plasma. The power supply typically operates in the 13.56 MHz international scientific and medical band. Sputtering with RF power can be performed at low gas pressures and this reduces the gas contamination in the growing film. Despite its advantages, the deposition rate is unfortunately low. The ferroelectric and tantalum based films described in this thesis were grown by RF sputtering [III, IV, VI]. The pulsed-DC technique combines the advantages of DC and RF sputtering, i.e. a high deposition rate and the ability to deposit from insulating targets. This technique uses an asymmetric bipolar square waveform operating at 50–250 kHz. The frequency, the pulse duration (duty cycle), and the relative pulse heights can be optimized depending on the target material. It is a popular method for the growth of high-quality piezoelectric AlN films [V, 22–32].

The magnetron sputtering process requires the generation of energetic ions which are responsible for the dislodgement of atoms from a deposition target. Prior to sputtering, the system is first evacuated to a base pressure of 10^{-6} to 10^{-8} mbar. Then the sputter gas is introduced at a constant flow that provides a low

and stable process pressure of 1–30 µbar. During operation, an electric field between the target and a substrate holder contains the hot electron cloud. The magnetic field causes the electrons to move along spiral-like paths and their collision with gas atoms leads to ionization. The argon ions are accelerated towards the negatively biased target where they dislodge the target atoms. The atoms subsequently travel from the target to the substrate and a film is formed through adsorption and adatom diffusion processes. Magnetron sputtering is a very versatile deposition method. The material selection is practically unlimited. Magnetron-sputtered films can exhibit excellent uniformity over large areas. The film properties can also be tailored by changing the deposition parameters such as substrate temperature, target-to-substrate distance, target power and composition, and process gas mixture and total sputter pressure. Moreover, the bombardment of the substrate with energetic particles can be enhanced by using a substrate bias during the deposition process. The bombardment improves adatoms mobility and removes loose bonds which under certain conditions results in an improved film quality. The intrinsic stress of the growing film is also strongly affected by the application of a substrate bias. Typically, the compressive stress increases with substrate bias. Sputtering power affects the deposition rate and film morphology. The substrate temperature has a strong effect on the degree of film crystallization and the density of film defects. During reactive sputtering, the process gas mixture determines the film stoichiometry. Magnetron-sputtered thin films are mostly polycrystalline in nature, however, with a proper seed layer and optimized deposition process high quality films can be obtained.

Reactive magnetron sputtering has been used in this study for the deposition of Ta_2O_5, Ta_2N, AlN, and BST films [III, IV, V, VI]. During this process a thin film is grown from a metallic or compound (oxide, nitride or carbide) target in a reactive atmosphere. In the latter case, the reactive gas is used to maintain the oxygen or nitrogen stoichiometry in the growing film. Reactive sputtering using metallic targets has some advantages over the sputtering from a compound target. Namely, metallic targets are cheaper and easier to manufacture and also cooling of metallic targets is more efficient and hence higher sputtering power can be used. On the other hand, the stoichiometry of a film grown from a compound target is more easily tailored.

The compound formation reaction may take place on the target, at the substrate, or in the vapor phase between target and substrate. Reactive sputtering can be operated in three modes, namely the metallic, transition and compound modes. The mode is determined by the process pressure, partial pressure of the

reactive gas, and sputtering power. To monitor the sputtering mode, the deposition rate, process pressure, and target voltage can be used. As a small amount of the reactive gas is introduced into the chamber, the deposition rate and target voltage decrease slightly. The process operates at the metallic mode and the deposited films are metal rich. The transition mode is reached when the deposition rate and target voltage changes become significant with increasing reactive gas partial pressure. In this mode, the rate of compound formation is competing against the sputtering rate on the target. As the compound coverage area increases, the sputtering rate and reactive gas consumption decrease. This, in turn, increases the partial pressure of the reactive gas and further reduces the sputtering rate. Finally the target voltage, deposition rate, and pressure drop suddenly indicating a transition to the compound mode or so-called target poisoning state. High quality films are generally sputtered at the reactive gas flow rate before drastic changes in the plasma parameters. In addition, hysteresis between the different operating modes does occur because the target voltage and deposition rate do not follow the same path upon a decrease of the reactive gas partial pressure. Reactive sputtering of thin compound films is a complex process and it is a demanding task to achieve reproducibility.

2.2 Thin film characterization

The films and multilayer structures were studied using different analytical techniques and device characterization methods. The crystallographic properties of the films were analyzed using x-ray diffraction (XRD) [I–VI]. The surface morphology was inspected by several techniques including optical microscopy, scanning electron microscopy (SEM) [I–VI], and atomic force microscopy (AFM) [I–VI]. The film thickness was measured using surface profilometry, cross-sectional SEM, and reflectometry. Also, transmission electron microscopy (TEM) was exploited for more detailed cross-sectional examinations of the thin films structures [I]. The surface profilometer was also used to analyze intrinsic residual film stress. The elemental composition of the films was determined with Rutherford back scattering (RBS) [III, IV, VI]. The electrical characteristics of the fabricated films were conducted by the fabrication of suitable test structures and the analysis of their DC- and AC-field properties.

2.2.1 Scanning electron microscopy

The surface and cross-section of the samples were examined utilizing scanning electron microscopy (SEM). The instrument used for the analysis was a LEO 1560 field emission SEM. The equipment offers a high lateral and vertical resolution and under optimum conditions features down to one nanometer can be imaged. In SEM an electron beam is focused on the specimen and backscattered or secondary electrons emitted from the surface are detected. The electrons that interact with the surface atoms provide information on the topography and composition of the sample. Electrons that are backscattered escape deeper from the sample and thus image formed by them exhibits compositional contrast and lower image resolution. On the other hand high-resolution images are formed with the secondary electrons that escape from the top few nanometers of the sample.

2.2.2 Transmission electron microscopy

Transmission electron microscopy (TEM) was applied to study the cross-section and film interfaces of the samples. The equipment used was a JEOL JEM-2010F which is capable of 0.19 nm structural resolution. In the technique, a beam of electrons is interacting with an extremely thin specimen. Part of the beam permeates through and the electrons are projected onto a screen below the sample. Contrast in TEM arises from mass and thickness variations in the sample. Thus, specimen preparation is a crucial part of TEM. In order to get samples less than 100 nm in thickness a combination of mechanical, chemical, and ion beam thinning steps is carried out. TEM provides morphology and crystallographic information of the studied sample in a cross-section geometry with very high resolution.

2.2.3 Atomic force microscopy

The surface morphology of the samples was examined by atomic force microscopy (AFM). In the technique, a sample is probed using a sharp AFM tip with a diameter of about 10 nm at the end of cantilever. The tip is scanned across a surface and the cantilever deflection due to surface topography is detected. A digital Instruments DI3100 AFM in tapping mode using 300 kHz silicon tips

was used in this study. The surface roughness of the samples was extracted from the measurements using the Nanoscope III software.

2.2.4 X-ray diffraction

X-ray diffraction (XRD) was used to characterize the crystalline properties of the films. The XRD analysis was performed using a Panalytical X'pert pro MRD diffractometer with Cu Kα radiation. In this technique, the studied sample is exposed to short wavelength X-rays. The radiation is diffracted from the sample and detected. The incident and reflection angles are coupled and accurately determined with goniometers during the diffraction scan. A diffraction pattern is developed when a crystalline film with repeating arrangement of atoms is irradiated with X-rays and the Bragg diffraction conditions are satisfied. To study the films, the XRD was operated in two modes. The lattice parameters, preferential film orientation, and lattice distortion were extracted from θ–2θ scan in which the incident and reflection angles are the same. Rocking curve measurements with a fixed detector angle were used to study the degree of grain alignment along the substrate normal. In addition, small angle diffraction i.e. X-ray reflectivity (XRR), measurements were exploited to determine the film thickness.

2.2.5 Rutherford backscattering spectroscopy

The elemental composition of the films was quantified using Rutherford backscattering spectroscopy (RBS). In this technique, a sample is irradiated with high-energy ions, usually alpha particles. The incident ions are backscattered due to collisions with atoms in the film. The energy loss is analyzed and from that the atomic masses of the elements in the film can be calculated. Unfortunately, small amounts of light elements in the sample are difficult to detect. The practical accuracy of the analysis is within a few atomic-percent. The instrument used in this study was a NEC pelletron 5SDH-2 tandem accelerator (2 MeV). The RBS measurements were quantified using a GISA 3.99 simulation program.

2.2.6 Electrical characterization

The test structures that were fabricated included patterned discrete TaN resistors, Ta_2O_5 capacitors, and ferroelectric capacitors and piezoelectric resonators with continuous bottom electrodes. The sheet resistances of the metallic and TaN

films were measured using a four-point probe technique. The temperature range in the TaN resistivity measurements was from -50 to 200 °C. The measurement was carried out using a Cascade Microtech probe station equipped with a temperature controlled shuck and a Hewlett Packard 34401A multimeter. The parallel-plate ferroelectric and Ta_2O_5 capacitors were measured from 40 Hz to 110 MHz frequency with an Agilent 4294A precision impedance analyzer with Cascade microprobes. In addition, the low-frequency properties of the ferroelectric capacitor were characterized from a cryogenic temperature of 20 K to room temperature. High frequency properties of the Ta_2O_5, ferro-, and piezoelectric films were extracted from wafer level S-parameter measurements with a Hewlett Packard 8720D vector network analyzer (VNA) with Cascade Microtech ACP-40 wafer probes.

3. Electrodes for parallel-plate devices

For optimal electrical characteristics and low losses at GHz frequency, the parallel-plate device geometry is often used. Insulating or resistive ceramic films are generally deposited at high temperature and in a reactive atmosphere. Despite the ability to tailor the material properties by changing the deposition conditions, the substrate and seed layer also have a strong effect on the structural and electrical properties of thin film devices. In parallel-plate devices the bottom electrode not only acts as electrical contact but also as a seed layer for subsequent film growth. The selection is therefore based on two main considerations: High electrical quality factor (*Q*-value) for high frequency applications and compatibility with high-quality ceramic film growth processes. At high frequencies the electrode quality factor depend on frequency as $Q_{ele} \sim 1/f$. In addition, it is also strongly influenced by the resistance and thickness of the electrodes [1–6]. The relevant properties of potential electrode materials are summarized in Table 1. Ag, Al, Au, Cu, and some refractory metals possess low resistivity and are thus the best candidates for high-frequency applications. Moreover, for high conductivity the electrode must be thermally stable, i.e. no reactions must take place between the bottom electrode and the ceramic film during high-temperature deposition in a reactive atmosphere.

Table 1. Properties of potential electrode materials.

Metal	Crystal structure	Resistivity (μΩcm)	CTE* ppm/°C	Density (g/cm^3)	Acoustic velocity (m/s)	Young's modulus (GPa)	Melting point (°C)	Work function (eV)[33]
Ag	fcc	1.59	18.9	10.5	2600	83	962	4.26
Al	fcc	2.65	23.1	2.7	5100	70	660	4.28
Au	fcc	2.35	14.2	19.3	1740	78	1064	5.1
Cu	fcc	1.67	16.5	8.9	3570	130	1085	4.65
Ir	fcc	5.3	6.4	22.7	4825	528	2466	5.27
Mo	bcc	5.2	4.8	10.3	6190	329	2623	4.6
Ni	fcc	6.84	13.4	8.9	4970	200	1455	5.15
Pd	fcc	10.8	11.8	12.0	3070	121	1555	5.12
Pt	fcc	10.6	8.8	21.1	2680	168	1769	5.65
Ru	hex	7.1	6.4	12.4	5970	447	2334	4.71
Ti	bcc	42.0	8.6	4.5	4140	116	1668	4.33
W	bcc	5.65	4.5	19.3	5174	411	3422	4.55

* Coefficient of thermal expansion

Figure 1(a) schematically illustrates the parallel-plate device geometry. In this geometry, the ceramic thin film is sandwiched between a bottom and top electrode. Coplanar interdigital capacitors without bottom electrode are a viable alternative for the parallel-plate geometry as it is easier to fabricate (see Fig. 1(b)). However, disadvantages of this design include lower capacitance, reduced tunability (large fringing electric field in the air between the electrodes), and the requirement of much higher tuning voltages due to a larger distance between the electrodes.

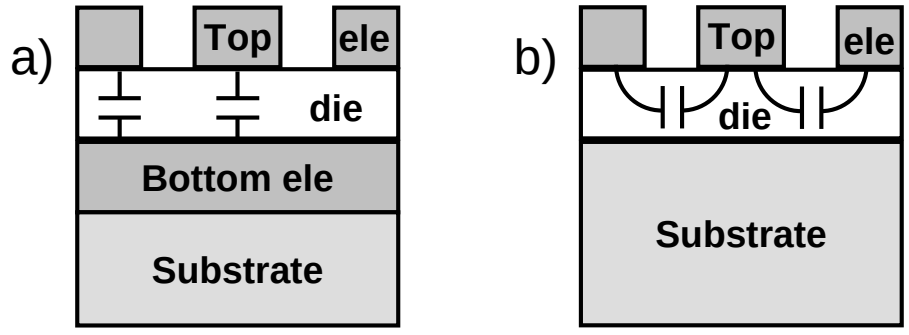

Figure 1. Illustration of (a) the parallel-plate and (b) coplanar geometry for capacitive devices.

To evaluate the high frequency losses of capacitive thin film devices an equivalent circuit of a resistor in series with a capacitor is generally used. The loss is sometimes expressed as the loss tangent ($\tan\delta$). The inverse of this is the quality factor (Q-value). It represents the ratio of stored energy to the average energy that is dissipated during device operation. In other words, the device Q_{tot} is the ratio of the measured reactance and resistance. Q_{tot} includes losses caused by the dielectric film Q_{die} and the conducting electrodes Q_{ele}. The total Q-value of the capacitor can be written as

$$\frac{1}{Q_{tot}} = \frac{1}{Q_{die}} + \frac{1}{Q_{ele}}. \tag{1}$$

At low frequency, the total Q-value is controlled by a combination of losses in the electrodes and the dielectric film [34, 35]. As the frequency is increased a steep decline in Q-value is generally observed due to a decrease of Q_{ele} [1–6]. The losses caused by the electrodes are approximated by:

$$Q_{ele} = \frac{1}{\omega CR}, \tag{2}$$

Where ω is the angular frequency i.e. $2\pi f$, C is the capacitance of the device, and R is the electrode resistance,

$$R = NR_s = N\frac{\rho}{d_{ele}}. \tag{3}$$

The capacitance of the structure is

$$C = \frac{\varepsilon_0 \varepsilon_r A}{d_{die}}. \tag{4}$$

The effect on the total *Q*-value, caused by the electrodes, is estimated by

$$Q_{ele} = \frac{d_{die} d_{ele}}{\omega \varepsilon_0 \varepsilon_r A N \rho}, \tag{5}$$

where d_{die} is the thickness of the dielectric film, d_{ele} is the electrode thickness, ε_r is the relative dielectric constant, ε_0 is the permittivity of free space (8.854×10^{-12} F/m), A is the electrode plate area, $N=l/w$ is the number of squares in the electrodes (the ratio of the total length l and electrode width w), and ρ is the resistivity of the electrode material. To increase the electrode quality factor, one could increase the electrode thickness (d_{ele}) or use an electrode material with low electrical resistivity (ρ). In addition, it is important to note that the electrode loss also depends on the geometry of the device [1, 34–37].

To estimate how much the electrodes affect the total device *Q*-value, a typical 30×30 μm^2 capacitor structure equipped with Cu electrodes and a RF probe with a pitch of 150 μm is used as an example (N = 5 squares). The calculated total quality factor (Q_{tot}) in the frequency range of 0.01 to 100 GHz is shown in Fig. 2. A capacitance of 3.9 pF (insulator thickness 750 nm with ε_r of 370) was used in these calculations. Moreover, it was assumed that the quality factor of the dielectric (Q_{die}) does not depend on frequency.

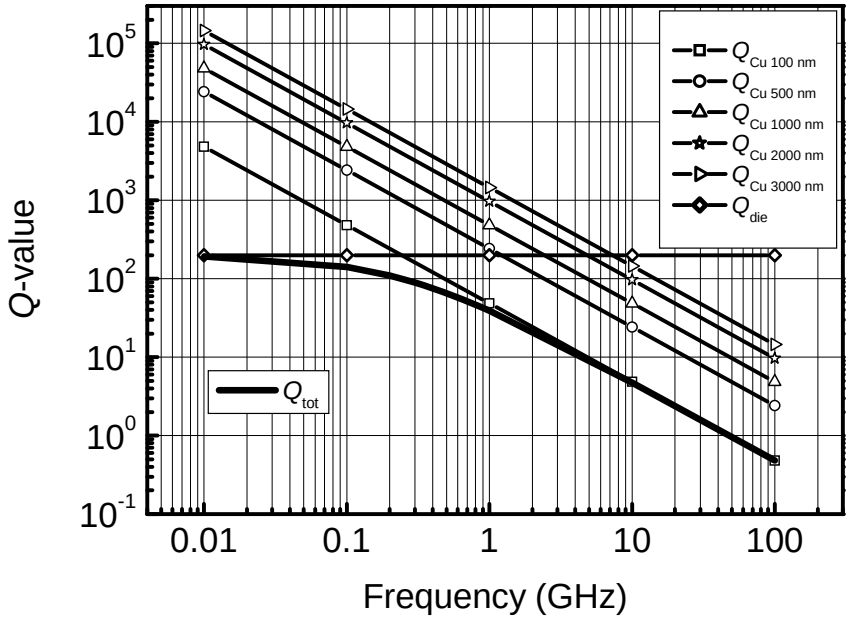

Figure 2. Calculated electrode (Q_{ele}), dielectric (Q_{die}) and total quality factors (Q_{tot}) as a function of frequency for a 3.9 pF capacitor with 100 nm thick Cu electrodes. Q_{ele} for different electrode thicknesses is also illustrated.

The solid line represents the total *Q*-value for a capacitor with 100 nm thick Cu electrodes. This simple calculation illustrates that the device *Q*-value is dominated by Q_{die} at low (MHz) frequency and that the Q_{ele} becomes dominant at GHz frequencies.

The same imaginary capacitive structure can be used to estimate the effect of the electrode material on the device *Q*-value. Using bulk resistivities and an electrode thickness of 1000 nm we calculated Q_{tot} and Q_{ele} for a frequency of 1 GHz. The results for Au, Cu, Mo, and Pt are listed in Table 2.

Table 2. Estimated influence of electrode material on the total device *Q*-values, Q_{tot} (Q_{ele}), for a 3.9 pF capacitor with an electrode thickness of 1000 nm at 1 GHz frequency.

	Material			
	Au	Cu	Mo	Pt
$Q_{tot}(Q_{ele})$	127(345)	142(485)	88(156)	55(76)

In conclusion, to minimize the losses of high-frequency devices, the electrodes should be fabricated from highly conductive metals such as Cu or Au. Moreover, the device quality factor can be improved by an increase of the electrode thickness. An additional phenomenon that should be taken into account at high frequencies is the so-called skin effect.

This effect reflects a concentration of current within a thin layer at the surface of a conductor and as it reduces the effective thickness of the electrodes it results in a further reduction of the quality factor. The current density decreases exponentially with depth d from the surface towards the core of the electrode. This exponential decay $e^{-\alpha d}$ is characterized by the decay constant α. The skin depth can be expressed as [38]

$$\delta = \frac{1}{\alpha} = \sqrt{\frac{2\rho}{\omega\mu}}, \tag{6}$$

where μ is the magnetic permeability, i.e. $4\pi 10^{-7}$ H/m for the non-magnetic materials listed in Table 1. The skin depth is the distance at which the current density is reaching $1/e$ (37%) of the current density at the surface. Figure 3 illustrates the skin depth for various metals as a function of frequency.

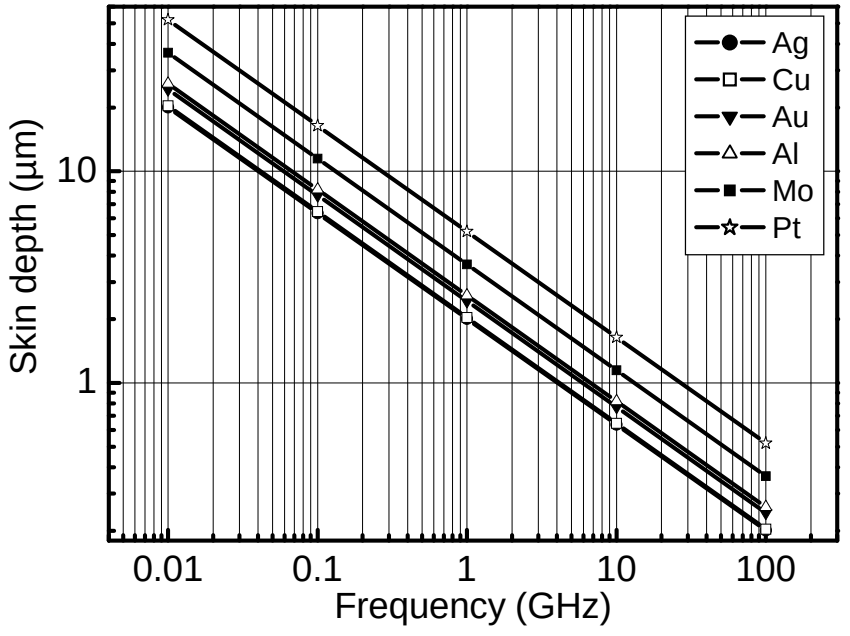

Figure 3. Skin depth of various materials as a function of frequency.

As observed in Fig. 3 the skin depth decreases with the conductivity of the electrode material. If $d_{ele} << \delta$ the electrical resistance (R) remains practically constant at microwave frequencies. However, the electrode resistance depends strongly on frequency when $d_{ele} \geq \delta$ due to the influence of the skin effect. For Cu, the second best conductor, the skin depth is 2.1 and 0.9 μm at 1 and 5 GHz. Making Cu electrode > 1 μm at 5 GHz only improves Q_{ele} a little.

Despite the ability to tailor material properties by thin film technology, the properties of thin films are usually inferior to their bulk analogs. The bulk resistivities of potential electrode materials are in the range of 1.59–10.6 μΩcm (Table 1). However, the resistivities of thin films with impurities, grain boundaries, surface roughness, and surface scattering tend to be considerable larger [39]. As a consequence the actual resistivity of electrodes strongly correlates with their thickness. Figure 4 shows an example for a Cu thin film grown on thermally oxidized silicon wafer with a 10 nm TiW adhesion layer.

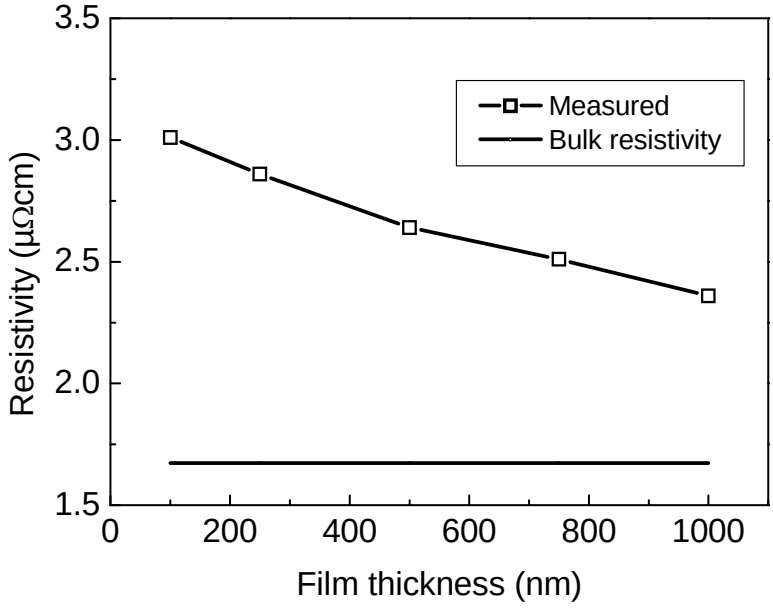

Figure 4. Resistivity of a Cu thin film (with a 10 nm TiW adhesion layer) as a function of film thickness.

The measured resistivity value at a typical electrode thickness of 500 nm is 2.64 μΩcm, which is 58 % higher than the Cu bulk value. Even for films as thick as 1-μm, the resistivity is larger than the bulk analog. Annealing [39] and proper seeding [40] can reduce the resistivity of electrodes to a certain extent. A further increase of the electrode thickness is problematic for magnetron-sputtered films due to a build-up of film stress and the potential exfoliation of the electrode. This also increases the demand for frequent maintenance of the sputter system and therefore electroplating of electrodes must be considered instead.

Besides the electrical properties of electrode material, the thermal and chemical stability of the device stack are also crucial. The harsh deposition conditions of ceramic films restrict the selection of bottom electrode materials. The bottom electrode should not only provide a good template for high-quality ceramic film growth, but it should also be able to withstand the high deposition temperature and reactive atmosphere during the ceramic deposition process. Noble metals such as Au and Pt are resistant to corrosion and therefore they are potential electrode materials. Some other materials such as Ir and Ru form self-passivating conductive oxides (IrO_2 and RuO_2) in O_2 atmosphere. However, evolving pas-

sivating oxide layer hinder the use of Ir and Ru in RF parallel-plate device applications due to parasitic capacitance caused by the oxide layer between electrode and the ceramic. In addition, conductive oxides such as RuO_2, IrO_2, RhO_2, OsO_2, ReO_2, $BaRuO_3$ $SrRuO_3$, $YBa_2Cu_3O_7$, and $(La,Sr)CoO_3$ have been used as electrodes in ferroelectric devices, but mostly for memory applications [41, 42] where their relatively high resistivity is less important. All highly conducting metals with a face-centered cubic (fcc) structure (Cu, Au, Al, and Ag) melt at rather low temperature. This makes them quite unstable during ceramic film deposition. As a rule of thumb if the processing temperature exceeds 33–50 % of the melting temperature, on a Kelvin scale, recrystallization and grain growth is expected to occur. When taking the high processing temperatures into account, Ag and Al can be excluded, while Cu and Au are borderline cases. On the other hand, refractory metals such as Mo and W endure high temperatures, but are prone to oxidation.

Low-loss high frequency devices require highly conducting electrodes. Cu is the most promising candidate for RF applications because of its high conductivity, low cost, high electromigration resistance, and patterning properties. According to literature, Cu has been successfully applied to varactor structures [I, 43]. In this study, the ceramic film was directly deposited onto the Cu electrode. To accommodate this with limited deterioration of the electrode properties a diffusion barrier (e.g. a thin Al-Ti film) must be used [43]. Additionally, devices equipped with high-temperature superconductor (HTS) electrodes and $SrTiO_3$ have been realized for space applications [14].The state-of-the-art bottom electrode for ferroelectric parallel-plate capacitors consist of a thick Pt [44] layer or Pt/Au bi-layer [3, 5]. Pure Au electrodes have also been used for oxide films with high dielectric constant [35].

Au or a combination of Au and Pt would be an ideal bottom electrode due to its high conductivity, chemical inertness, and ease of patterning with potassium iodide or cyanide based etchants. However, Au recrystallizes and grain growth occurs at high processing temperatures. This makes Au and Au/Pt structures unstable for ferroelectric capacitor applications. Furthermore, layered structures of Au and Pt are soluble at high temperatures [46].

In Au thin films a large scale surface morphology change occurs at high annealing temperatures [II]. Grains can grow up to a few micrometers in diameter. Figure 5 shows an AFM picture of a magnetron sputtered 500-nm Au film on Si/SiO_2/10nmTiW substrate as-deposited and after annealing in a vacuum furnace for one hour at 650 °C.

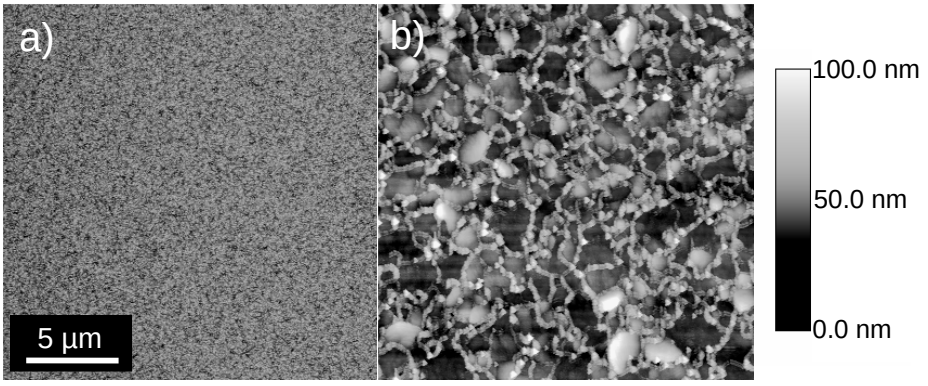

Figure 5. (a) AFM image of an as-deposited 500 nm thick Au film. (b) AFM image of the same film after annealing in a vacuum furnace for 1 h at 650 °C [II]. The film was grown at room temperature.

Drastic surface texture changes can be observed. During annealing the RMS roughness of the Au surface increased from 5.1 to 12.5 nm. The coarsening and growth of grains can be explained by a recovery and recrystallization (secondary grain growth) of the Au film.

Pt is the most widely used electrode metal in thin film oxide based devices because of its chemical inertness and stability at high temperatures. Barium strontium titanate capacitors with Pt electrodes have shown favorable leakage characteristics [42] due to the formation of a Schottky contact at the Pt/BST interface. However, the relatively high resistivity of Pt films requires the use of thick electrodes to limit losses at high frequency. The problem with thick Pt is its stability at high temperatures. To study the behavior of Pt at elevated temperatures, a relatively thick Pt electrode (750 nm) was sputtered onto a Si/SiO_2 substrate with a thin TiW (5 nm) adhesion layer. The sample was annealed in an open-end furnace at 650 °C for 30 minutes. Annealing in the air furnace resulted in gigantic grain growth as illustrated by the SEM images of Fig. 6.

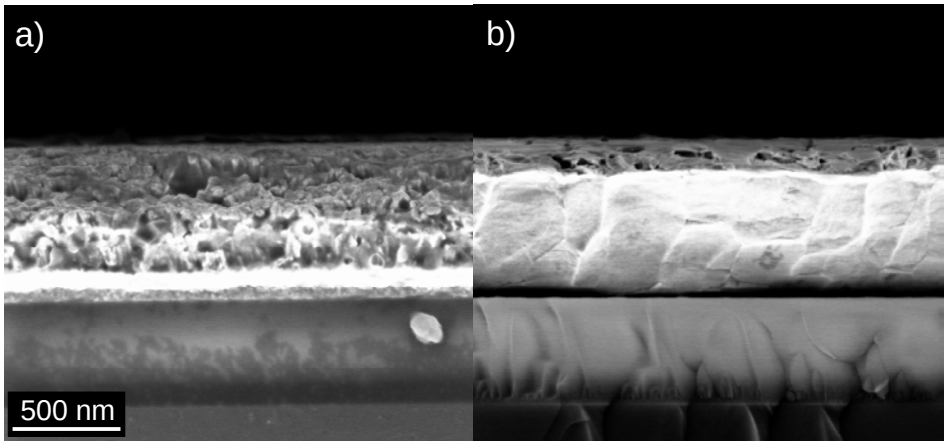

Figure 6. SEM images of (a) as-deposited thick Pt electrode and (b) the same electrode after annealing at 650 °C for 30 minutes in an open-end furnace. The film was grown at room temperature.

The resistivity of the Pt electrode decreased from 17.3 μΩcm in the as-deposited state to 13.5 μΩcm after annealing. This decrease of film resistivity can be attributed to a reduction of crystal defects and grain growth during the annealing process. However, grain growth also roughens the electrode surface and this might lead to excess leakage current in actual devices. Additionally, compressive stress in the Pt film should be eluded since it can inflict hillock formation and shorted device structures [47]. Stauf et al. embedded conducting stabilization layers of TiAlN or IrO_2 into the Pt layer to realize bottom electrodes as thick as 2 μm for ferroelectric varactors [44]. Another challenge with thick Pt electrodes is their integration into devices because of their chemical inertness. Wet etching of Pt is possible only with heated Aqua regia, a mixture of hydrochloric acid and nitric acid. Reactive ion etching (RIE) of platinum is difficult due to the non-existence of readily generated volatile etching products at low temperature. In order to form lithographically defined patterns ion milling is the predominant etching method and this limits the workable electrode thickness.

In addition, while platinum itself is resistant to oxidation, it is highly permeable to oxygen [48–50]. Due to its inherently poor adhesion to oxide films, an adhesion layer such as Cr, Ti or TiW must be used. However, diffusion and oxidation of the adhesion layer can cause grain growth and hillock formation in Pt films [47]. The problem can be overcome by using an electrode stack consisting

of a platinum layer together with an additional oxide diffusion barrier [51, 52] or by using an other adhesion layer that is less prone to oxidation [53]. On the other hand, migration of Ti through the Pt bottom electrode has played an important role as nucleation sites for BST film growth [50]. Thin Pt electrodes can be used without an adhesion layer [II]. In this case the adhesion can be improved by *in situ* Ar ion bombardment of the substrate prior to Pt deposition. The use of thin Pt bottom electrodes is, however, not ideal as it tends to compromise the structural quality of the ceramic film and leads to large losses at high frequencies.

High melting point refractory metals such as W and Mo are thermally stable materials at ceramic film processing temperatures. Also, their resistivities are suitable for RF device applications. A disadvantage of Mo and W is their affinity to oxygen. Therefore, refractory metal electrodes must be covered with a diffusion barrier against oxidation [II, 45]. Mo electrodes with a sacrificial metallic diffusion barrier of Al-Ti were studied in publication II. The Al-Ti layer (75 nm in thickness) was co-sputtered from pure elemental targets in a 1:1 ratio which results in nanocrystalline or amorphous films [54]. The samples were annealed in an air furnace for 30 min at 650 °C. Figure 7 shows cross-sectional SEM images of the 75 nm thick Al-Ti barrier layer on Mo in the as-deposited state and after annealing.

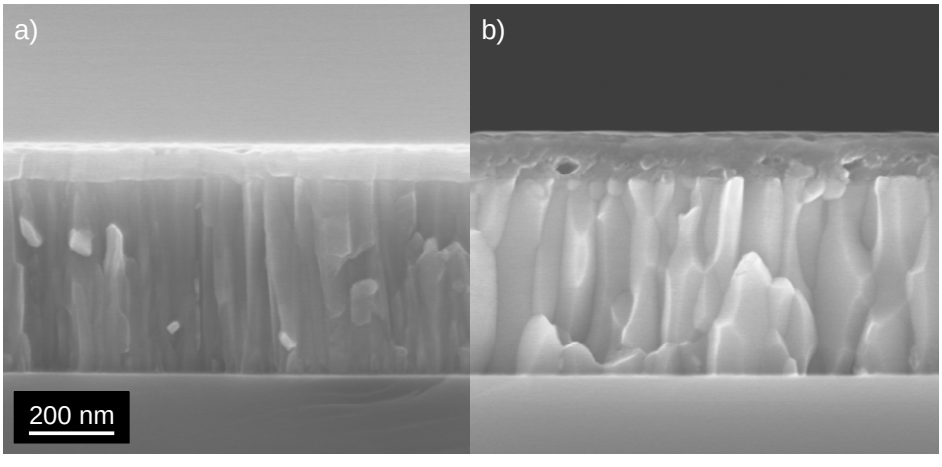

Figure 7. Cross-sectional SEM image of a sacrificial (Al-Ti) diffusion barrier on Mo in (a) the as-deposited state and (b) after annealing in air furnace for 30 min at 650 °C [II]. The films were grown at room temperature.

During annealing, the Al-Ti layer reacted with oxygen leaving the Mo film underneath intact. Swelling of the Al-Ti layer took place during the oxidation process. Although the resistivity of the barrier did not change (verified by four-point measurements) during the annealing process, the resistivity of the as-deposited film (177 μΩcm) was already too high for low-loss RF applications. Stable Mo electrodes can also be fabricated using insulating diffusion barriers. However, these layers add a parasitic capacitance to the parallel-plate capacitor structure and thereby degrade the overall device performance.

Moreover, a close match of the coefficient of thermal expansion (CTE) of the substrate, bottom electrode, and growing ceramic film are required for high-quality device structures. BST thin films have been deposited on expensive single crystal substrates such as MgO, $LaAlO_3$, and Al_2O_3. CTE values for the above-mentioned substrates are 11.15, 12.5, and 6.0 ppm/°C, respectively. The CTE values are 9.0 ppm/°C for Pt and 8–11 ppm/°C for BST. Because of the good lattice and CTE matches, high quality epitaxial Pt and ferroelectric thin films can be grown on these substrates. However, the use of Si substrates has many benefits including price, good thermal conductivity, stability and the availability of fabrication technologies. The major drawback in using Si is its low CTE value of 2.49 ppm/°C. The CTE for SiO_2 is 0.55 ppm/°C and the values for potential electrode materials are listed in Table 1. A difference in the CTE of the silicon substrate, the thermal SiO_2 layer, the bottom electrode, and the ferroelectric film strains the film lattice when the substrate is cooled down from the ceramic deposition conditions to room temperature [16, 55, 56]. In the worst case, cracking and adhesion loss of the films can occur.

Finally, the deposition parameters for all metallic electrode films used in this study are summarized in Table 3. The film deposition was carried out in the Von Ardenne cluster sputtering tool described in Chapter 2.1.2.

Table 3. Overview of the deposition parameters of studied metallic materials for electrodes.

	Pt	Mo	Cu	Au	Al-Ti †
Sputtering power (W)	800	1000	1000	800	400/390
Power supply (RF/DC)	RF	DC	DC	RF	DC
Argon flow (sccm)	50	16	30	30	Both 68%
Pressure (μbar)	3.3	0.9	6.9	2.0	† Diffusion barrier

In addition, the diffusion barrier structure mentioned in the Table was grown in a custom-build co-sputtering system.

4. Layer transfer

As outlined in the previous chapter, the quality factor of a parallel-plate device is limited by electrode losses at GHz frequencies. To limit the detrimental effects of the electrodes they should be highly conductive and thick. Integration of ceramic films with low-loss metallic electrodes has been problematic. The main issues relate to the high deposition temperature, typically 600–800 °C, and the reactive atmosphere that are required for the growth of crystalline ceramic films. Due to these harsh deposition conditions the metallic bottom electrode is degrading during ceramic film growth and this has made the manufacturing of parallel-plate structure very challenging. To overcome these problems we, for the first time, used a layer transfer method to fabricate parallel-plate devices with low-loss electrodes. This method, which involves the transfer of the ceramic film and the electrode structure from an auxiliary substrate to a device substrate, has many advantages. The main feature of this fabrication technique is a separation of the electrode and seed layer functions. As a result, the electrodes are no longer exposed to the harsh deposition conditions of the ceramic films and consequently any highly conducting material can be selected as low-loss electrode. Fabrication of RF parallel-plate devices with very high *Q*-values at GHz frequencies becomes therefore feasible.

A schematic illustration of the layer transfer process flow is shown in Fig. 8. A ceramic film is grown on a first (auxiliary) substrate (e.g. Si and a suitable seed layer). The substrate and potentially the seed layer will be later removed and therefore their selection can be exclusively based on their ability to promote high-quality ceramic film growth. Next, the bottom electrode is deposited on top of the ceramic film. The electrode material can be rather freely selected, e.g. highly conducting Cu, Al, Ag or Au for low-loss applications. Since the deposition can be done at low temperatures (e.g. $T < 200$ ºC) and oxygen is highly bound to the already grown ceramic film, the metal electrodes do not degrade by

oxygen nor temperature. The bottom metal electrode can also be patterned. Then, a buffer layer is grown (e.g. thick SiO_2) and planarized. The role of the buffer layer is to allow wafer bonding to a second substrate (e.g. quartz). Alternatively, the buffer layer can consist of an adhesive or polymer film (e.g. BCB, polyimide). After this, the ceramic film and bottom electrode are transferred to a second substrate by wafer bonding. The auxiliary substrate is removed after wafer bonding. Possible methods include (i) chemical wet-etching of Si (HF + HNO_3 + CH_3COOH) or (ii) chemical-mechanical thinning (grinding, polishing) followed by plasma etching (e.g inductively coupled plasma (ICP) etcher or deep reactive ion etcher (DRIE)). Key aspect in removal of the auxiliary substrate is the etch selectivity between the different layers. Finally, the top electrode is deposited. As for the bottom electrode, the material of the top electrode can be freely selected.

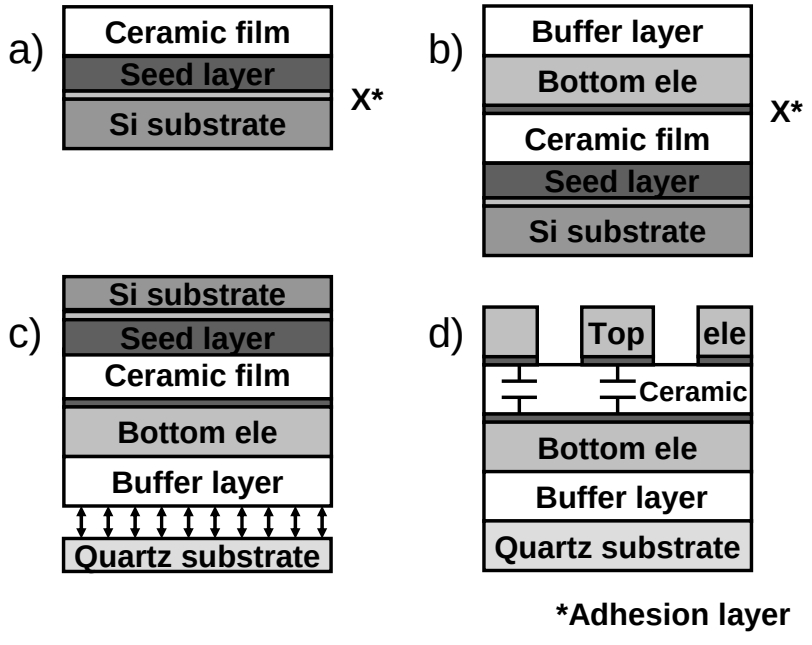

Figure 8. Schematic illustration of the fabrication process for ceramic parallel-plate devices using the layer transfer method.

Successful wafer bonding is crucial for the layer transfer method. Wafer bonding technologies have been used for integrated circuits (IC) and microelectromechanical systems (MEMS). Well known examples include Smartcut™ and other

silicon-on-insulator (SOI) based technologies. The wide variety of wafer bonding techniques includes direct bonding (high/low temperature), metallic bonding, anodic bonding, and adhesive and polymer bonding [57, 58].

Adhesive bonding, direct wafer bonding, and Au-Au bonding have been investigated for the fabrication of ceramic parallel-plate devices. Wafer bonding with polymer adhesives utilizes an intermediate layer to bond different materials. The process is versatile, robust, simple, low cost, and insensitive to surface topography [58]. The disadvantages include a limited temperature and chemical durability, and poor mechanical properties, especially hardness. The Young's modulus of polymers is at least two orders of magnitudes smaller than those of ceramics, silicon, and metals. This will complicate the integration of fragile thin films with a substrate that yields under pressure. As an example, the imprint of probe tips on a substrate with a 500 nm $Ba_{0.5}Sr_{0.5}TiO_3$ with TiW 30 nm/Cu 500 nm/TiW 10 nm multilayer stack is shown in Fig. 9. The stack was transferred onto an epoxy polymer film on a quartz wafer and the sacrificial silicon wafer was subsequently etched using RIE. The underlying epoxy polymer film yields even under the application of minor probe tip pressure and this damages the parallel-plate device structures. As a result, the BST/electrode structure is pierced and electrically shorted. The use of polymer films to transfer ceramic layers is therefore troublesome.

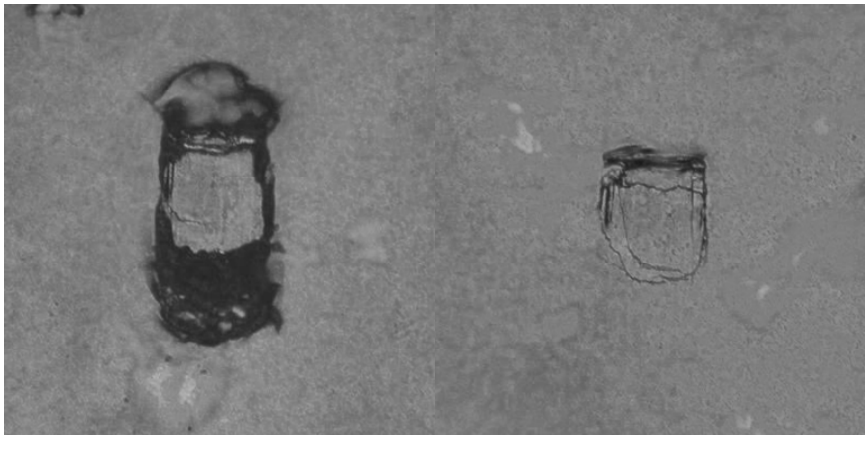

Figure 9. Optical (50X) microscope images of the imprint of RF probe tips on BST/TiW/Cu/TiW/epoxy/quartz substrate with different contact forces.

Au is an attractive material for solid phase bonding because of its resistance to oxidation and its self-diffusion characteristics. The process, however, is highly

surface sensitive. Wafer bonding with thermocompression of Au can be performed at low temperatures ~300 °C under 4 MPa of pressure [59]. Layer transfer of single crystalline dielectric thin films via H^+ and He^+ ion implantation and high temperature exfoliation onto a silicon-based substrates has been investigated [60, 61]. By combining these two techniques i.e. ion implantation into a single crystalline substrate and Au-Au bonding, a high quality ferroelectric film with highly conductive electrodes on a RF compatible substrate could be realized. In our experiment, H^+ and He^+ ions were implanted into a single crystalline 10×10 mm^2 $SrTiO_3$ (STO) substrate. After this, we deposited Au onto the STO and onto a sapphire device substrate. Bonding of the substrates was conducted at 300 °C and to exfoliate the STO surface layer we heated the substrates *in situ* to 400 °C. This resulted in a 670 nm single crystal STO film on a sapphire substrate with a 1 µm thick Au bottom electrode. Figure 10 shows an optical microscope image of the exfoliated STO thin film on Au. After this, a 1 µm top Cu electrode was fabricated using photolithography and lift-off.

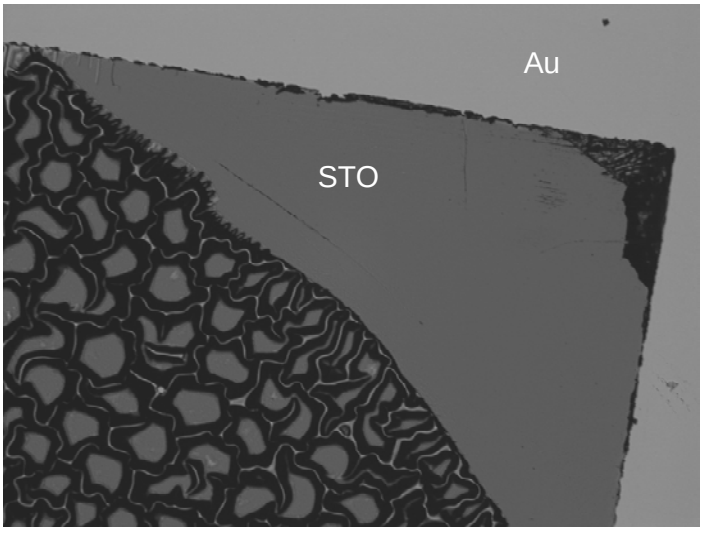

Figure 10. An optical (10X) microscope image of an exfoliated single crystal $SrTiO_3$ thin film on Au.

The exfoliated STO film was attached only at the corners of the sapphire substrate due to a large STO substrate curvature. The unbonded film is wrinkled as illustrated by the image of Fig. 10. The transferred single crystal STO film on a 2 µm thick Au bottom electrode showed exceptional field-strength up to 40 V,

a zero-field relative permittivity of 155, and tunability of ~25 %. However, the *Q*-value of the device was poor (~40) even at low MHz frequencies. The high dielectric loss in the STO film is probably due to defects generated by the ion implantation process [62]. The implantation damage can be significantly recovered with the annealing at relatively high temperature [62], but this will undoubtedly deteriorate the electrode structures. The practical use of layer-transferred single crystal films is also limited by the high substrate costs and small substrate area.

A wide variety of materials can be bonded directly without intermediate adhesives or external force [63]. Metal-ferroelectric-silicon structures based on direct wafer bonding have been demonstrated by Alexe et al. [64]. The ferroelectric-semiconductor heterostucture in their study was adapted to memory and integrated detector applications.

In this thesis, direct wafer bonding was used to transfer ferroelectric and piezoelectric films and suitable electrode structure onto RF compatible substrates. In publication I layer transfer of ferroelectric $Pb_xSr_{1-x}TiO_3$ (PST) thin films and thick Cu bottom electrodes by direct wafer bonding onto RF compatible quartz substrate is demonstrated. In this study, first a 660 nm thick PST film was deposited using sol-gel onto a 100 mm silicon wafer with a 100 nm Pt/10 nm Ti/SiO_2 seed layer. Several spin coating/drying cycles of the precursor solution were conducted at room temperature (spin coating) and 200 °C (drying) and the resulting PST film was crystallized by annealing at 650 °C for 15 min. For adhesion purposes we then sputtered a thin TiW layer (10 nm) before depositing a 650 nm thick Cu bottom electrode and another TiW film (20 nm). Next, a 1000 nm thick SiO_2 was grown by plasma enhanced chemical vapor deposition and this was planarized by chemical-mechanical polishing. Layer transfer to a 100 mm quartz substrate was achieved by vacuum bonding at room temperature and the bond was subsequently strengthened by heating at 200 °C for 2 h in vacuum. The auxiliary silicon substrate was then thinned by grinding to <100 µm which then peeled off along the Pt/PST interface. Finally, a 650 nm thick Cu top electrode with a 20 nm TiW adhesion layer was sputtered and patterned by photolithography for electrical characterization.

Irregularities between the bonding interfaces hinder the critical bonding process. A release coverage of 75–80% was achieved on the PST sample. Full coverage/yield is possible with modern bonding techniques, however, due to particles on the PST film the active area remained limited. Figure 11 shows a bright-field

TEM image of the PST parallel-plate capacitor with highly conducting Cu bottom and top electrodes.

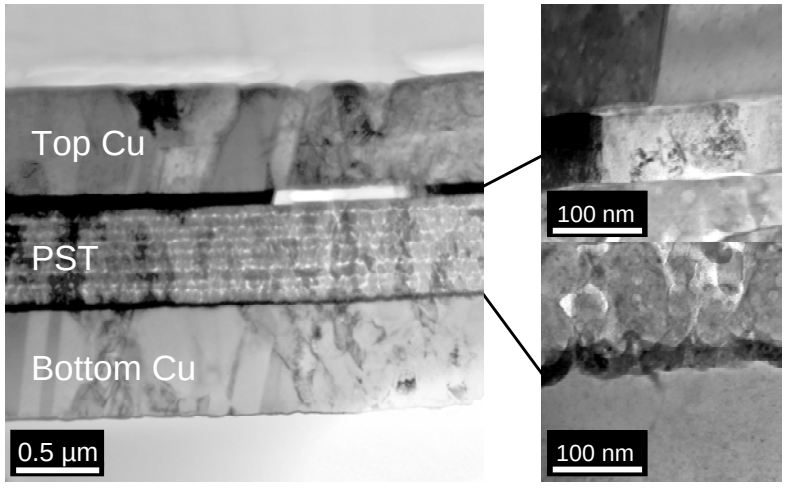

Figure 11. Bright-field TEM image of the Cu/PST/Cu parallel-plate capacitor structure. Enlargements on the right side show TEM images of the Cu top electrode/PST and PST/Cu bottom electrode interfaces [I].

More detailed bright-field TEM images of the electrode/oxide interfaces are shown in the right panels of Fig. 11. The Cu bottom electrode and the PST film are separated by a rough interlayer with dark contrast. This layer corresponds to TiW that, when grown on top of the relatively rough ferroelectric film, diffused into the PST grains. In contrast, the interface between the PST film and the Cu top electrode is abrupt. This clearly indicates that the original PST/Pt interface on the sacrificial substrate was smooth. Moreover, subsequent sputtering of the Cu top electrode on the exposed PST film did not introduce pronounced interface roughness. Finally, the mechanical stability of the multilayer stack was ensured with standard tape tests. As mentioned in the previous chapter, the PST film and Cu electrodes both contribute to the total dielectric loss of the Cu/PST/Cu parallel-plate capacitors. To a first approximation the measured loss tangent consists of Q_{PST} and Q_{ele} as illustrated by Eq. 1. Since the electrode loss scales with the size of the capacitor, the quality factors of the PST film and electrodes can be determined separately by measuring the loss tangents as a function of capacitor area [6]. The experimental results at a frequency of 1 GHz are shown in Fig. 12. In this case, $\tan\delta = 1/Q_{PST} + A/(Q_{ele}A)$ and fitting the data gives $Q_{\mathrm{PST}}=26$ and $Q_{ele}A=3.79\times10^5$ µm^2. The quality factor of the electrodes is very

large, which is mainly due to the use of highly conductive Cu on both sides of the PST film. For a capacitor with a diameter of 10 µm, for example, it is nearly 5000 at 1 GHz.

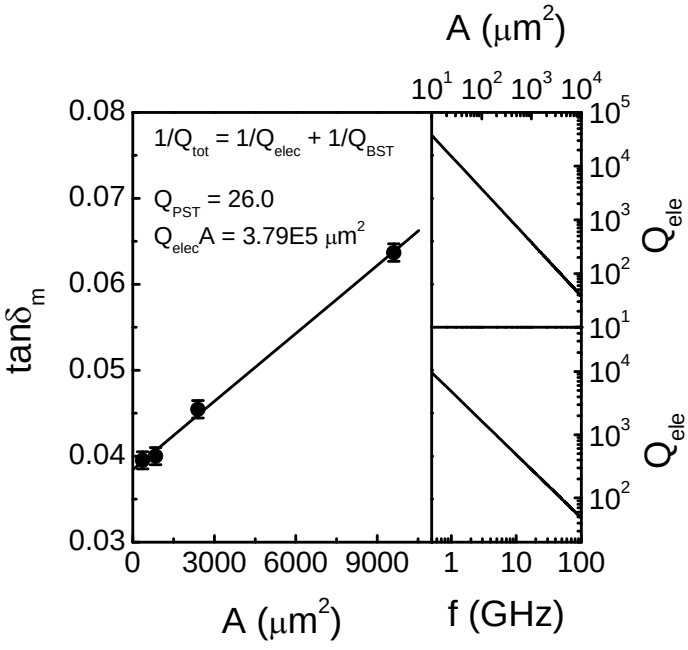

Figure 12. Measured dielectric loss ($\tan\delta_m$) as a function of Cu/PST/Cu capacitor area at 1 GHz. The upper right and lower right graphs show the variation of the electrode quality factor as a function of capacitor size (at 1 GHz) and frequency (for a capacitor with a diameter of 10 µm). These dependencies follow from the experimentally determined value of $Q_{ele}A=3.79\times10^5$ µm² [I].

Moreover, as $Q_{ele} \sim 1/f$, the quality factor of the electrodes is anticipated to remain larger than 100 up to a frequency of about 50 GHz (see lower right panel in Fig. 12). The low Q_{PST} is partly due to the ferroelectric character of this film at room temperature. Piezoelectric transformations, domain wall movement, and scattering by spontaneous polarization thus contribute to the dielectric loss. Other possible sources of loss are the boundaries between the randomized PST grains and the metal/oxide interface layers. These results clearly demonstrate the potential of the layer transfer method for the fabrication of ferroelectric parallel-plate capacitors with low-loss electrodes, which holds a great promise for microwave device applications. In addition, it enables measurements of true losses in ferroelectric films at high frequencies.

5. Ferroelectric parallel-plate capacitors

Ferroelectrics are a class of materials which posses a switchable spontaneous electric polarization P_S. The polarization is caused by ion displacement in the crystal lattice and switching can be induced by the application of an electric field E across the material. The most promising and utilized ferroelectrics for tunable capacitor applications are materials which have a perovskite crystal structure ($A^{2+}B^{4+}O_3$). Barium strontium titanate (BST) is one of the most intensively studied materials, whose lattice structure changes as a function of temperature. Figure 13 shows the typical temperature dependence of the dielectric permittivity and lattice structure of $Ba_{0.25}Sr_{0.75}TiO_3$. The point where the material undergoes a solid-to-solid (martensitic) phase transition (permittivity peak) is called the Curie temperature T_C. Below the transition temperature, the material is in the ferroelectric (polar) state with a tetragonal lattice structure and exhibits a spontaneous polarization. The spontaneous polarization is caused by the natural displacement of the highly charged Ti cation into a non-centrosymmetrical position. Switching the polarization by an applied electric field causes hysteresis. Above the Curie temperature a centrosymmetrical (cubic non-polar) i.e. paraelectric state exists without hysteresis.

Barium strontium titanate ($Ba_xSr_{1-x}TiO_3$) is a solid solution of barium titanate ($BaTiO_3$) and strontium titanate ($SrTiO_3$). By mixing ferroelectric and paraelectric materials the dielectric properties can be tailored towards particular applications. The Curie temperature of $BaTiO_3$ can be shifted from 120 °C to below room temperature by substituting Ba with Sr in the crystal lattice. The decrease of T_C is approximately 3.4 K per mol% of Sr [41]. BST exhibits paraelectric behavior at room temperature if the Sr content exceeds 35 mol% [65]. $Ba_{0.25}Sr_{0.75}TiO_3$, on the other hand, undergoes a ferroelectric to paraelectric phase transition at low temperatures as illustrated by the maxima in the relative dielectric permittivity versus temperature curves of Fig. 13.

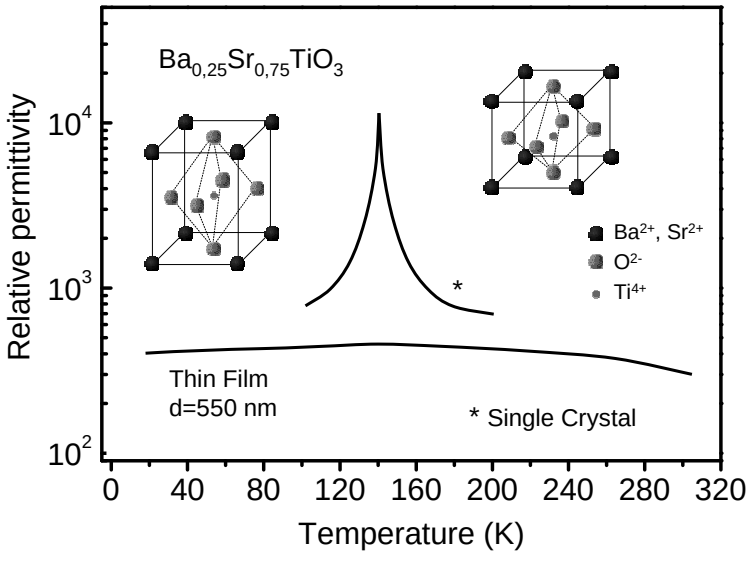

Figure 13. Comparison of bulk vs. thin film properties of $Ba_{0.25}Sr_{0.75}TiO_3$.

For BST single crystals, the ferroelectric to paraelectric phase transition is considerably sharper than in thin films and the dielectric permittivity in the paraelectric state is described by the Curie-Weiss law

$$\varepsilon_r(T) = \frac{C_W}{(T - T_C)}, \tag{7}$$

where C_W is the Curie-Weiss constant and T_C is the Curie temperature. The reduction of dielectric permittivity in thin films can be attributed to small grain size, defects, interfacial capacitance, and residual stress [66].

For tunable device applications such as varactors, it is desirable to have maximum dielectric permittivity and thus tunability in combination with small dielectric loss at room temperature. The tunability is maximized near the Curie temperature. However, at this temperature the dielectric loss tends to be large due to a transition to the ferroelectric phase. Another major problem with the existence of polar regions in the ceramic film is hysteresis, which is an unwanted property for tunable RF applications.

At microwave frequencies the dielectric loss of BST films are intrinsic and extrinsic in nature. The intrinsic loss is present also in ideal BST crystals and represents the highest achievable performance of a ferroelectric device [12]. The

intrinsic loss arises from the interaction between AC fields and phonons in the ceramic material [12]. These interactions include the three-quantum, four-quantum and quasi-Debye mechanisms [12]. On the other hand, material defects in composition or structure cause extrinsic losses. Important extrinsic loss mechanisms include charge defects, relaxation, and polar regions where the quasi-Debye mechanism is active [12]. AC field induced motion of charged defects results in the generation of acoustic waves. This loss mechanism is important in thin films with a high defect density. For good quality films the dielectric loss decreases with applied electric field [14]. In addition, domain wall movement causes hysteresis which converts electric power into heat. The lower loss paraelectric phase is thus highly desirable for high frequency applications. At very high frequencies (> 10 GHz) the paraelectric phase may, however, not always be required [67]. In spite of all this, ferroelectric device losses at GHz frequencies are often dominated by the ohmic losses in the electrodes as described in chapter 3.

In the desired paraelectric phase the perovskite has a cubic lattice structure in which the oxygen anions occupy the cell faces and the A cations (Ba and Sr) the corners. The Ti cation is located in the centre of the oxygen octahedron as illustrated in Fig. 13. An applied electric field displaces the Ti ions from their zero-field position within the octahedron and this changes the capacitance. The dielectric permittivity decreases (tunes) as a function of this displacement. A typical capacitance vs. voltage tuning curve for a magnetron-sputtered $Ba_{0.25}Sr_{0.75}TiO_3$ parallel-plate capacitor with 100 nm Pt electrodes is shown in Fig. 14.

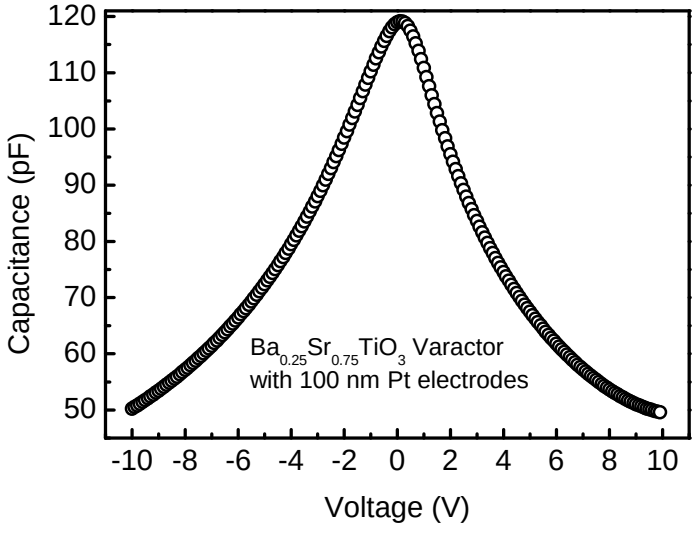

Figure 14. Bias voltage dependence of the capacitance of a Pt/$Ba_{0.25}Sr_{0.75}TiO_3$/Pt parallel-plate capacitor at 10 MHz. The BST film of 330 nm in thickness was deposited at 650 °C with a substrate bias of 60 V.

The tunability depends on many factors such as the Ba/Sr ratio, temperature, and film strain [12]. In this thesis, we define the tunability as

$$n_r = 1 - \frac{1}{n} = \frac{\varepsilon(0) - \varepsilon(V)}{\varepsilon(0)}. \tag{8}$$

Here ε(0) is the zero-bias permittivity and ε(V) is the permittivity measured at bias voltage V. The tuning curve of Fig. 14 corresponds to a dielectric tunability of 55 % at 10 V.

The field-dependent polarization properties of paraelectric thin films have shown great promise for the design of high frequency tunable thin film devices such as phase shifters, tunable filters, voltage controlled oscillator (VCO), frequency modulators, parametric amplifiers, and tunable power dividers [12]. The other potential competing technologies are semiconductor varactors and micro-electro-mechanical systems (MEMS) varactors [68]. Semiconductor varactors are fast, small, and highly tunable. Additionally, they can be readily integrated with other circuits. However, they suffer from large losses at RF frequencies, junction noise, poor linearity, and relatively high tuning voltages. Furthermore,

they are expensive. MEMS varactors have high Q-values at RF frequencies. Linearity and power handling are also good. The drawbacks of MEMS varactors are slow switching speed, low tunability, high operation bias voltage, and packaging costs. BST, on the other hand, has attractive properties for high frequency applications including:

- good tunability of about 50–70%
- fast polarization response < 1 ns
- high breakdown field
- *Q*-value of more than 100 at GHz frequencies
- low cost.

For devices, the dielectric response of BST films can be tailored by changing the process parameters. The dependence of the dielectric properties on deposition temperature, growth rate, process pressure, film composition, and film thickness have been reported [16–20]. The properties of BST thin films tend to differ considerably from their bulk analogs due to grain size effects, charged defects, the formation of interface layers, and the build-up of lattice strain [VI, 9, 12, 14].

The deposition of BST films onto various metallic electrodes generally results in polycrystalline films. (100), (110), and (111) peaks and higher order reflections can often be distinguished in XRD scans [VI, 55, 69–71]. By controlling deposition parameters such as temperature, substrate bias, and total deposition pressure, the relative contribution of the different crystalline orientations can be changed. In particular, the number of (100) and (200) grains increases at the expense of (110) BST grains when the deposition temperature [69, 71] or substrate bias [VI] is increased. On the other hand, an increase of the deposition pressure results in more (110) and (200) textured BST films [72]. In addition, the commonly used Pt bottom electrodes exhibit a clear (111) texture and this tends to promote BST (111) film growth [VI, 55]. Finally, Lee et al. showed that the orientation of BST films also depends on the thickness of the Ti adhesion layer underneath the Pt [50].

The film composition is also strongly affected by the deposition parameters. A slight deviation in the Ba/Sr ratio, which determines the Curie point, is not crucial because the temperature-dependent phase transition of thin films is rather broad (see Fig. 13). A more important factor affecting the dielectric properties of the BST films is the (Ba+Sr)/Ti ratio. The influence of Ti nonstoichiometry is emphasized in literature [17–19, 56, 73]. Im et al. reported that the Ba/Sr and (Ba+Sr)/Ti ratios could be adjusted by the total sputter pressure [17]. The O_2/Ar

ratio did not strongly affect the composition in their study. The films with a large (Ba+Sr)/Ti ratio exhibited a large relative dielectric permittivity of ~500, a low Q-value of ~100, and a high tunability of ~74%. On the contrary, BST films with a high Ti concentration showed a low relative permittivity (~300), a high Q-value of ~200, and a low tunability of ~50%. The measurements were conducted at a frequency of 10 kHz.

Additionally, the dielectric properties of paraelectric films do deteriorate with decreasing film thickness [8, 16]. This is due to the presence of an interface "dead layers" [8, 16] with lower permittivity than the bulk of the film. The relative importance of the interface layers decreases for thicker ceramic films [8, 16].

For high-frequency applications, integration of high-quality ferroelectric films with highly conductive electrodes is required. Stauf et al. realized BST capacitors on Pt bottom electrodes as thick as 2 µm [44]. The dielectric constant was in the range of 150–400, depending on the film thickness. The *Q*-value of BST film was found to be over 150 at 100 MHz and a tunability of 50 % was achieved [44]. Composite metallization stacks of 1.5 µm W and 0.1 µm Ir have also been used for BST varactors [45]. A tunability of 50 % (~100 nm BST) and a *Q*-value of 143 between 100 Hz and 500 kHz were observed in this case [45]. $Ba_{0.25}Sr_{0.75}TiO_3$ varactors with a thick electrode (0.5 µm Au + 50 nm Pt) have shown *Q*-values of more than 100 up to 10 GHz in combination with a tunability of 40 % at 25 V [3]. The BST films exhibited a dielectric permittivity of 150 with a 300 nm thick BST [3]. Nguyen et al. introduced a state-of-the-art commercial MIM varactor with a ParaScan™ BST thin film. The *Q*-value was approximately 100 at 1 GHz with a tunability of 76 % at 27 V bias voltage [74]. Nonferroelectric $Bi_{1.5}Zn_{1.0}Nb_{1.5}O_7$ (BZN) thin films have also been investigated for high frequency varactor applications [2]. The BZN (~300 nm) devices with a 200-nm Pt bottom electrode showed 30 % tunability at 1 MV/cm, a dielectric constant of 180, and a *Q*-value of more than 100 at 20 GHz [36]. Fan et al. developed layered electrode structures of TiAl/Cu/Ta as a template for BST deposition [43]. A relatively high dielectric constant of 280 (160 nm BST) and a *Q*-value of 143 were achieved at 10 kHz with Cu-based electrodes.

In our study, we focused on the influence of substrate bias on the structural and dielectric properties of paraelectric thin films. Colliding ions transfer additional energy to the surface of the substrate when a substrate bias is used. With relative modest ion energies, surface rearrangement and densification might take place, while substantial energies can cause ion implantation, defect structures, and resputtering of the deposition material. Moreover, preferential resputtering

from the growing film can occur due to differences in the sticking coefficient of complex compounds.

The BST films were deposited onto thermally oxidized silicon substrates with a 50 nm Ti/100 nm Pt seed layer using RF magnetron sputtering from a $Ba_{0.25}Sr_{0.75}TiO_3$ target in a 3:1 Ar/O_2 atmosphere. During BST film growth, the substrate temperature was held at 650 ºC. To examine the influence of substrate bias during BST growth we deposited films with 0 V (floating), 20 V, 40 V, and 60 V applied bias voltage.

The application of substrate bias affects the surface morphology of the BST films as illustrated by the SEM images of Fig. 15.

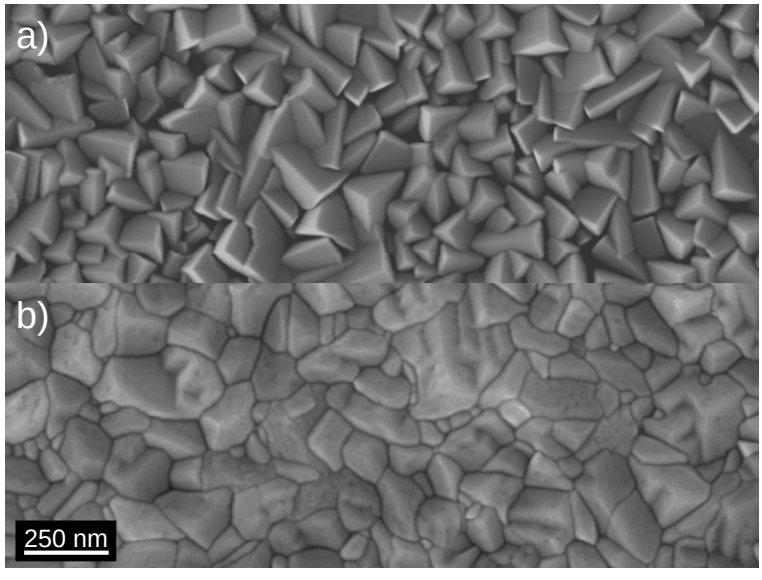

Figure 15. SEM images of the surface morphology for $Ba_{0.25}Sr_{0.75}TiO_3$ films grown (a) without substrate bias and (b) with a substrate bias of 40 V [VI].

If no substrate bias is applied during RF magnetron sputtering, a loose columnar grain structure evolves with various crystalline orientations and clear facets at the surface. The application of a substrate bias provides additional energy to the growth process leading to a dense and nearly void free film, rounding of the evolving grain structure.

The polycrystalline nature of the BST film is confirmed by the XRD measurements shown in Fig. 16. BST (100), (110), (111), (211), and (310) can be distinguished for most films. In the case of 0 V substrate bias, the (200) peak

width is larger than at other bias values, which is possibly due to a small splitting between the BST (200) and the Pt (200) peaks. Substrate bias induced film stress cause peaks to shift in the XRD spectra. A complete overlap of the BST (200) and Pt (200) peaks is achieved when a substrate bias is used during film growth.

The relative contribution of the different crystalline orientations changes with applied substrate bias.

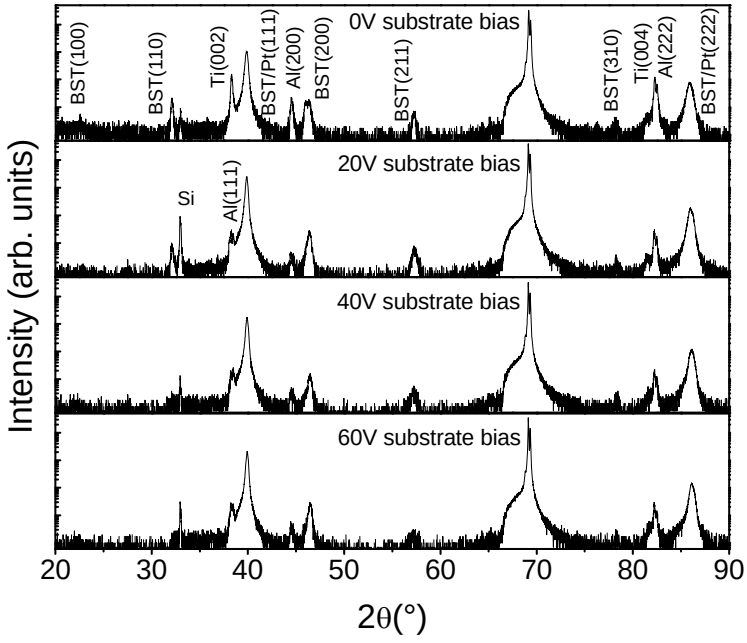

Figure 16. θ-2θ XRD scan of Pt/$Ba_{0.25}Sr_{0.75}TiO_3$/Al parallel-plate capacitor structures grown with different substrate bias during BST magnetron sputtering [VI].

In particular, the number of (100) and (111) grains increases at the expense of (110) and (211) BST grains. The preferential growth of (100) grains can be explained by the low surface free energy of the densely packed BST (100) plane. The application of a substrate bias provides additional energy to the growth process and this promotes the formation of energetically favorable crystalline orientations. Moreover, the Pt (111) bottom electrode induces a high degree of BST (111) film texture and the formation of (111) grains is more efficient when a substrate bias is applied during RF magnetron sputtering.

The growth of BST films on Ti/Pt seed layers at high temperatures normally induces lattice strain. First of all, a difference in the coefficient of thermal expansion (CTE) of the silicon substrate, the thermal SiO_2 layer, the Ti and Pt seed layers, and the BST film strains the BST lattice when the substrate is cooled from the deposition conditions (650 ºC in our experiments) to room temperature. Cooling after deposition is therefore expected to result in tensile in-plane and compressive out-of-plane BST film strain. Other factors that determine the strain state of the BST film include the lattice misfit with the Pt bottom electrode and deposition parameters such as substrate temperature, sputtering power and pressure, and substrate bias. Figure 17 summarizes the out-of-plane BST lattice distortion of grains with a (100) and (111) crystalline orientation relative to their bulk values as a function of applied substrate bias. The data of Fig. 17 were extracted from the shift of the BST (200) and (222) reflections to larger angles in the XRD $\theta - 2\theta$ scans. The BST film grown without applied bias exhibits a reduced out-of-plane lattice parameter (about -0.3% compared to bulk BST) and thus a tensile in-plane film strain. This agrees qualitatively with the difference in CTE values of the substrate material, seed layers, and BST film. The out-of-plane lattice parameter was about -0.6% smaller than the bulk BST value at high bias voltages (40 and 60 V).

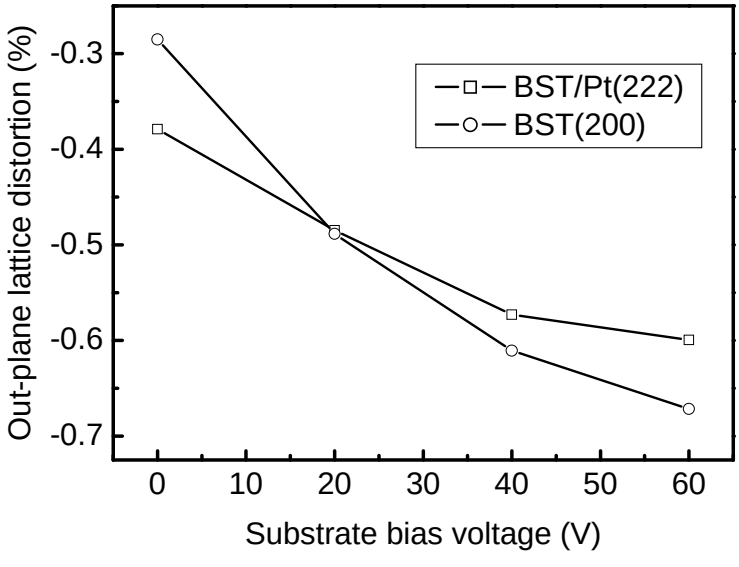

Figure 17. Out-of-plane lattice distortion relative to a bulk value of a_{BST} = 0.3930 nm for BST films grown with different substrate bias [VI].

The dielectric properties of BST films depend critically on the elemental composition. To determine how the substrate bias influences the film composition we conducted detailed RBS experiments. Figure 18 summarizes the Ba/Sr and (Ba+Sr)/Ti atomic ratios as inferred from fits to the RBS data.

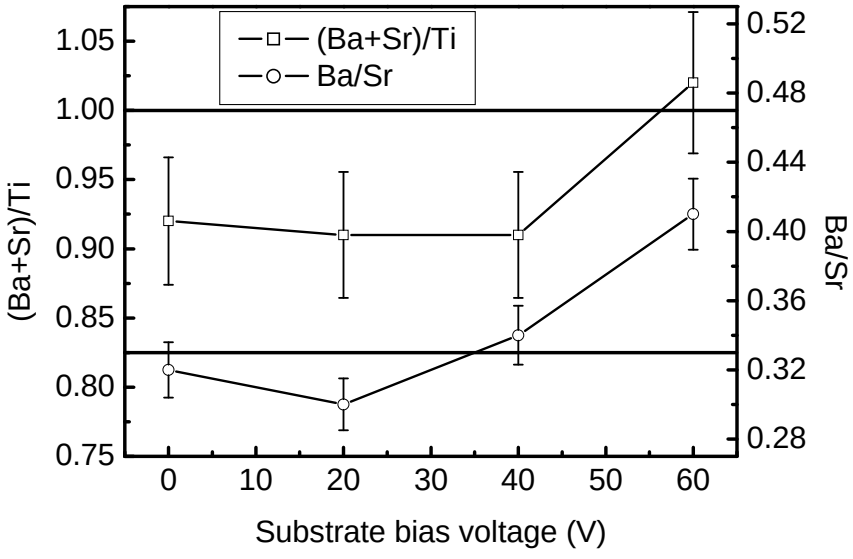

Figure 18. Influence of substrate bias on the Ba/Sr and (Ba+Sr)/Ti ratios of magnetron-sputtered films from a $Ba_{0.25}Sr_{0.75}TiO_3$ target. The lines indicate the Ba/Sr and (Ba+Sr)/Ti ratios of the magnetron sputter target [VI].

At low bias voltages ($\leq$ 40 V), the Ba/Sr ratio is about 1/3 which agrees well with the nominal composition of the BST sputter target. The (Ba + Sr)/Ti ratio, on the other hand, is only about 0.92 in these films. An abrupt change in the film composition occurs when the substrate bias voltage is increased from 40 V to 60 V. The Ba/Sr ratio in the BST film increases to about 0.41, which is considerably larger than the ratio of the sputter target. Moreover, the Ti non-stoichiometry almost completely disappears at 60 V substrate bias, i.e. the (Ba + Sr)/Ti ratio equals 1 within experimental error. Preferential resputtering from the growing BST film most likely explains the observed shift in film composition.

The BST films undergo a ferroelectric to paraelectric phase transition at low temperatures with broad maxima. The maximum of the dielectric permittivity shifts to higher temperatures if the BST films are sputtered onto a biased sub-

strate. The transition temperatures are 120 K (0 V), 140 K (20 V), 180 K (40 V), and 210 K (60 V). The observed shift of the ferroelectric to paraelectric phase transition to higher temperature with increasing substrate bias is at least partly explained by an increase of the Ba content due to preferential resputtering of Ti and Sr. The +60 K shift is also partly explained by an increase of the tensile in-plane film strain. Other groups have also reported an increase of the ferroelectric to paraelectric phase transition temperature with increasing mechanical strain for BST films [56, 66, 75, 76].

Figure 19 shows the electric field dependence of the relative dielectric permittivity of the Pt/$Ba_{0.25}Sr_{0.75}TiO_3$/Pt parallel-plate capacitors at 1 MHz. The zero-field dielectric permittivity increases non-monotonically with applied substrate bias during RF magnetron sputtering of the BST film. For a substrate bias of up to 40 V the increase of the dielectric permittivity is rather modest (from 350 to about 410).

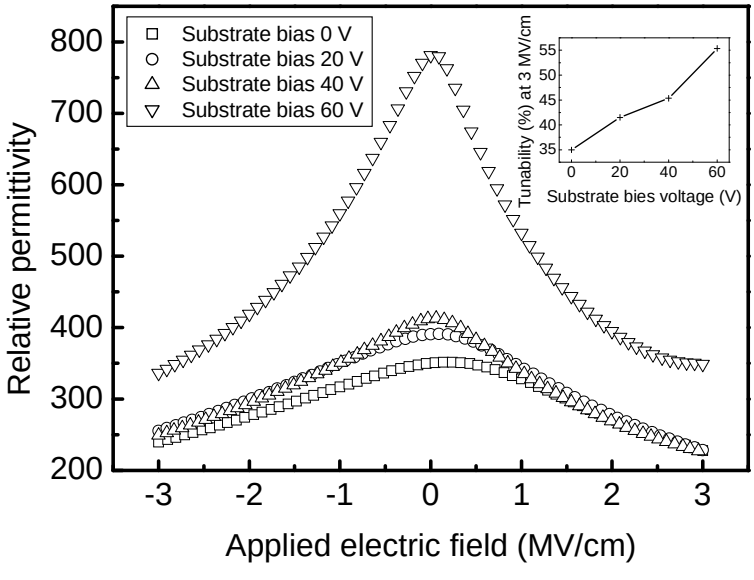

Figure 19. Electric-field dependence of the relative dielectric permittivity for $Ba_{0.25}Sr_{0.75}TiO_3$ films grown with different substrate bias. The data was collected at 1 MHz. The inset shows the dielectric tunability as a function of substrate bias [VI].

Increasing the substrate bias to 60 V drastically enhances the zero-field permittivity to 780. The dielectric tunability also increases with substrate bias voltage.

For the non-biased BST film, the tunability at an electric field of 3 MV/cm is 35% and it increases to 55% for a substrate bias of 60 V (see inset of Fig. 19). The Q-value of the different BST capacitors at 1 MHz is summarized in Fig. 20. The BST films grown without substrate bias and a bias of 20 V exhibit a large Q-value of about 200. Interestingly, the electric-field dependence of these two capacitors is different. A leakage current decreases the quality factor of the BST film grown without substrate bias above 1 MV/cm. No such effect is measured when a 20 V bias is used during BST sputtering. Instead, the quality factor increases with applied electric field and this is a clear indication of the quality and relatively low defect density of this BST film. This observation is also confirmed by measurements of the breakdown field, which is largest for BST films grown with a substrate bias of 20 V. The quality factor decreases for higher substrate bias. This is most likely due to defect structures that are created by high energy ion bombardment of the BST film during RF magnetron sputtering at elevated substrate bias.

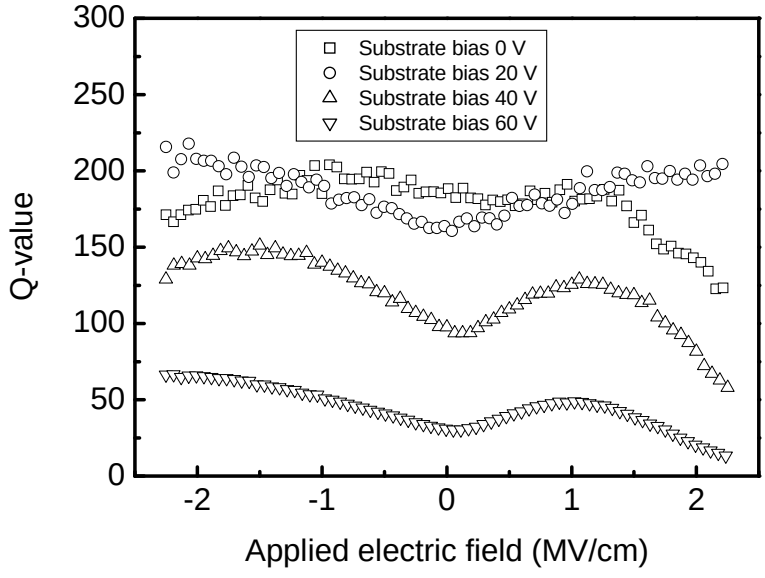

Figure 20. Q-value of Pt/BST/Pt parallel-plate capacitors at 1 MHz as a function of applied electric field and substrate bias [VI].

Dielectric properties such as permittivity, tunability, and loss of magnetron-sputtered BST films were thus significantly affected by the application of a substrate bias during deposition. The effects of the electrode material and electrode

thickness on the device *Q*-value at high frequency for BST-based capacitors were also tested. To do this, we used the layer transfer method as described in Chapter 4 to fabricate $Ba_{0.25}Sr_{0.75}TiO_3$ parallel-plate capacitors with Cu bottom and top electrodes. The BST film was deposited onto a 100 mm platinized silicon wafer at 650 °C. The resulted ferroelectric capacitor consisted of a Cu (1 µm) + TiW (20 nm) + Pt (50 nm) /BST (600 nm) / TiW (20 nm) + Cu (500 and 750 nm) + TiW (40 nm) thin film stack on a quartz substrate. The bottom Cu electrode was continuous and the top electrode was patterned using photolithography and lift-off processes. Moreover, to control the film quality a reference sample with a 100 nm Pt bottom electrode was grown. The *Q*-values of the devices were measured with an impedance analyzer at MHz range and a network analyzer was used to extract the *Q*-values from measured S_{11} scattering parameters up to GHz frequencies. Figure 21 shows the *Q*-value of the fabricated devices with the Pt and Cu bottom electrodes. In Fig. 21 the measurement is divided into two parts: the impedance analyzer measurement at low frequency which is then continued with data from the network analyzer at higher frequencies.

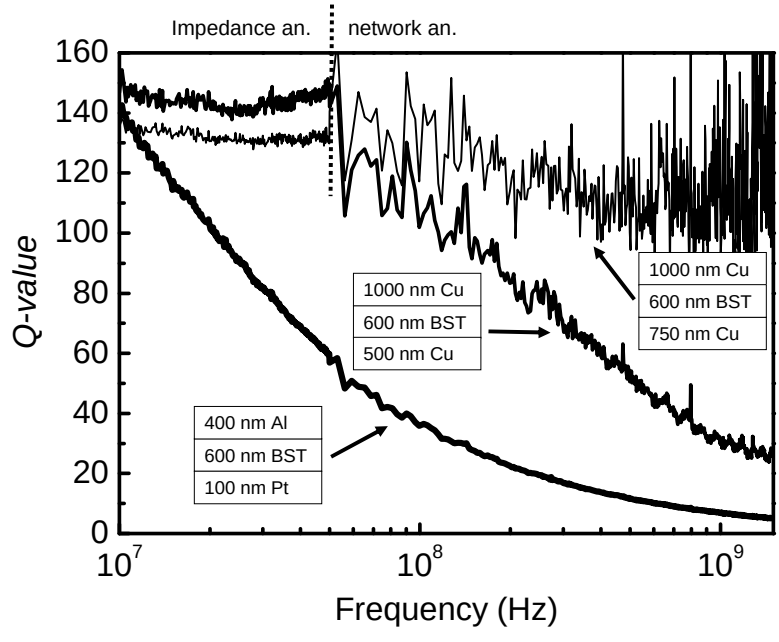

Figure 21. Q-value of 85×85 µm^2 $Ba_{0.25}Sr_{0.75}TiO_3$ parallel-plate devices with a capacitance of 32 pF.

The *Q*-value of the reference sample starts to decrease at low MHz frequencies due to electrode losses. At low frequencies, the electrode contribution is negligible when highly conductive electrodes are utilized and therefore the device properties resemble those of the paraelectric film. The samples with Cu electrodes exhibit a nearly constant *Q*-value up to almost 100 MHz. At higher frequencies, the *Q*-value is determined by a combination of electrode and dielectric film losses. Figure 21 clearly shows that by using highly conductive electrode materials and by increasing the electrode thickness the device *Q*-value can be enhanced at high frequencies. The layer transfer method enabled the fabrication of ferroelectric parallel-plate capacitors with a quality factor of about 100 at 1 GHz. This is among the best ferroelectric parallel-plate capacitor performance found in literature. Even better *Q*-values at higher frequencies could be reached by using smaller area electrodes as shown in Ref. [34]. We have also succesfully fabricated ferroelectric device structures based on BST with patterned 2 µm thick bottom Cu electrode. Unfortenately the device characterization was unfinished during the publication of this thesis.

Besides the obvious advantage of high-conductivity bottom and top electrodes, the layer transfer method also facilitates the use of microwave-compatible device substrates. Thick electrodes that are normally utilized to minimize substrate losses are therefore no longer a prerequisite for low-loss operation at high frequencies. In particular, silicon, a popular substrate choice for conventional parallel-plate capacitors, will contribute to dielectric losses if the electrode thickness is smaller than the electromagnetic penetration length or so-called skin depth.

6. AlN bulk acoustic wave resonators

Thin film RF filters can be constructed using capacitors and planar spiral inductors. However, the large size and low *Q*-value of the planar coils has hampered large-scale industrial applications. An alternative approach to achieve high-*Q* inductors for frequency controlled applications, without the use of a real inductor, is to convert the electrical signal into a mechanical vibration (sound) and utilize the resonance of the sound waves [31]. This is effectively accomplished by using piezoelectric materials. The two devices that utilize this principle are surface acoustic wave (SAW) filters and bulk acoustic wave (BAW) filters.

Commonly used SAW materials include single crystalline substrates of quartz (SiO_2), lithium tantalate ($LiTaO_3$) and lithium niobate ($LiNbO_3$). The SAW technology is based on acoustic (Rayleigh) waves which travel along the substrate surface between interdigital combfinger transducers. Frequency control is achieved by designing the lateral period of the electrode fingers. Finally, the acoustic energy is converted back into the electrical domain. The manufacturing of SAW structures is relatively straightforward and therefore it has become a popular technology for RF filter applications. However, practical devices are currently limited to 2.5 GHz due to the resolution of the optical lithography process that produces the required narrow linewidths and small gaps.

For frequencies up to 20 GHz, thin film bulk acoustic wave resonators are the technology of choice. Commonly used BAW materials include thin film aluminum nitride (AlN), zinc oxide (ZnO) and lead zirconate titanate (PZT). Table 4 shows the important material parameters for the piezoelectric thin films used in BAW applications. In a BAW resonator, a signal voltage across a piezoelectric layer excites an acoustic wave. In AlN film the Al and N atomic layer distance i.e. film thickness changes under an electric field and due to this movement the acoustic wave is launched. The wave is confined to oscillate between the air boundaries in a membrane type configuration or between a bottom acoustic mir-

ror and the air boundary in a solidly mounted resonator (SMR) configuration [77]. The piezolayer converts the mechanical vibration with a characteristic frequency back into an electric signal. Extremely little energy is radiated into the air in membrane-type BAW resonators and this results in potentially high *Q*-values. This is further promoted by the small number of layers that have to be fabricated. The major drawbacks are power handling and the brittleness of membranes. For SMR BAW devices the films are grown onto an acoustic mirror (reflector) to isolate the device from the substrate. The mirror consists of pairs of low/high acoustic impedance materials with a thickness that corresponds to a quarter of the acoustic wavelength at the operating frequency, typically ~650/750 nm alternating in pairs at 2 GHz. The choice of materials determines the number of pairs needed. Adequate isolation can for example be achieved when two pairs of high impedance W and low impedance material of SiO_2 are combined. Key benefits of BAW resonators include low power consumption, small size, low cost, high spectral purity, and sufficient stability.

Table 4. Comparison of piezoelectric materials for BAW applications [78].

Material	K^2 (%)	Dielectric constant ε_r	Acoustic velocity (m/s)	Dielectric loss
AlN	6.5	9.5	10400	very low
ZnO	7.5	9.2	6350	low
PZT	8–15	80–400	4000–6000	high

Key parameters that determine the response of a thin film BAW structure are the effective electro-acoustic coupling coefficient (K^2) which defines the degree of energy exchange between the electrical and mechanical domain and the maximum attainable bandwidth and the quality factor (Q), i.e. the losses of a filter. K^2 depends strongly on the quality of the piezoelectric film, the electrode configuration, and the substrate.

The electrical characterization of BAW resonators is generally performed by measuring the one-port scattering parameter S_{11} on wafer level. From the S_{11}, the input impedance Z_{in} is calculated using:

$$Z_{in} = \frac{1+S_{11}}{1-S_{11}} Z_0, \tag{9}$$

where Z_0 is the line impedance (50 Ω). The series and parallel resonance frequencies (f_s and f_p) can be determined from zero crossings of the impedance phase ϕ. The effective electro-acoustic coupling coefficient can then be calculated using [27]:

$$K^2 = \frac{\pi^2}{4}\frac{f_p - f_s}{f_s}. \tag{10}$$

The quality factors of the series and parallel resonances are given by [27]:

$$Q_{s,p} = \frac{\omega}{2}\left|\frac{d\phi}{d\omega}\right|_{\omega_s,\omega_p} \tag{11}$$

where ω is the angular frequency. Finally, a figure of merit (FoM) indicating resonators performance for low-loss wide bandwidth RF applications can be calculated using [79]:

$$FoM = K^2 \cdot \max(Q_s, Q_p). \tag{12}$$

For BAW filters in the 1–5 GHz range, the electro-acoustic coupling coefficient K^2 should be more than 6.5 [30, 79], the Q-value should exceed 1000 [79], and the figure of merit FoM should be at least 50 [29].

At present, AlN is predominantly used as piezoelectric material in BAW devices [22, 24, 25, 27, 32] as it exhibits good electro-acoustic coupling, it is very stable, non-toxic, environmentally friendly and compatible with microelectronic IC-processing. To fulfill the device requirements for e.g. mobile phone applications, the AlN film must be of very high quality [22, 24, 25, 77, 79, 80]. Material requirements include exact stoichiometry, hexagonal wurtzite crystallographic structure with a well-defined (002) orientation (see Fig. 22), and strict control over film stress and roughness. Growth of c-axis oriented AlN layers requires optimization of the deposition conditions and of substrate and seed layer combinations. Deposition methods that have been used to grow AlN include chemical vapor deposition (CVD), pulsed-laser deposition (PLD), molecular beam epitaxy (MPE), and RF magnetron sputtering. The dominating method today, however, is reactive pulsed-DC magnetron sputtering.

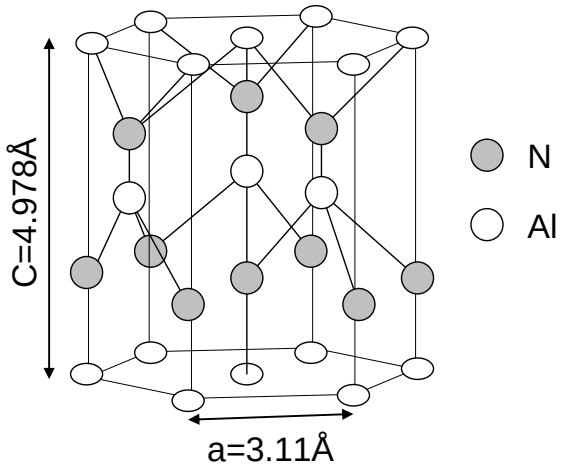

Figure 22. Schematic illustration of the wurtzite lattice structure of aluminum nitride.

The growth of high quality AlN is sensitive to very low levels of oxygen contamination [81]. Thermodynamically, Al reacts faster with oxygen than with nitrogen and the formation of unwanted Al_xO_y will deteriorate AlN columnar growth. Thus ultra high vacuum (UHV) with a base pressure of less than 1×10^{-8} mbar is required for the deposition of AlN films. Moreover, the AlN films should be grown at high sputter power to minimize oxygen incorporation.

For a good resonator response, the electrodes should have low electrical resistivity, small acoustic losses, and high acoustic impedance. The need for low resistivity electrode materials is related to the electrical losses as discussed in chapter 3. Moreover, as the bottom electrode serves as seed layer for piezoelectric film growth, it should also provide a high degree of crystalline texture, limited surface roughness, and proper chemical surface conditions. Finally, to constrain the acoustic waves between the electrodes a high acoustic impedance is required. The acoustic impedance is defined as

$$Z = \sqrt{\rho \times E}, \tag{13}$$

where ρ is the material density and E is Young's modulus. The most commonly used electrode materials are (111) oriented face centered cubic (fcc) metals such as Al, Pt and Ni [24, 27, 32, 77, 82–86], (110) oriented body centered cubic (bcc) materials like Mo and W [22, 24, 25, 27, 30, 82, 84, 85, 87–92], and hexagonal metals with a (002) orientation including Ti and Ru [25, 82, 84, 86].

For high-quality AlN growth, especially Mo bottom electrodes fulfill the device requirements including low resistivity, high-degree of (110) crystalline texture, high density and low surface roughness. The use of a low total sputtering pressure induces compressive residual stress and promotes a dense and smooth microstructure with uniform grain size [V, 85, 87, 93] and low resistivity [87, 93]. Low sputtering pressure also promotes a (110) film orientation [87, 93]. High sputtering power on the other hand, densifies the Mo film and this also results in a smooth surface morphology [87]. Besides the influence of the Mo deposition parameters, the crystallinity and morphology of the Mo electrode is also greatly affected by the choice of seed layer material. Matsumoto et al. and Kamohara et al. studied the influence of AlN seed layers on the growth of Mo electrodes [88, 90]. Both the Mo film smoothness and quality of the (110) crystalline orientation were substantially enhanced by the use of an AlN seed layer as compared to films that were directly deposited onto Si or SiO_2 substrates. Akiyama et al. examined a metallic Au/Ti seeding bi-layer for Mo electrodes [89]. AlN deposited onto the Mo/Au/Ti layer was superior to Mo/Ag/Ti and Mo/Pt/Ti. In addition, metallic seed layers such as Ti [V, 87, 91], Ta [91], Cr [91], TiW (10/90 wt-%) [V], and Ni [V] have been investigated for Mo.

In our study, we focused on the growth of high-quality AlN onto Mo bottom electrodes using pulsed-DC magnetron sputtering. In these experiments we particularly investigated the influence of thin seed layers on the growth of the Mo electrode and the piezoelectric AlN layer. The different seed layers were TiW, Ni, and Ti. The aim was to obtain a dense and smooth microstructure with uniform grain size for optimal electro-acoustic performance. To optimize the growth of Mo, several deposition parameters for the seed layers were varied, in particular the film thickness and magnetron sputtering power. The growth conditions of the Mo electrodes were found to have little effect and consequently were kept constant throughout the experiments. SEM images of the Mo surface morphology deposited onto different optimized seed layers are shown in Fig. 23. The optimal seed layer thickness and sputtering power for the three systems are 20 nm/500 W (Ti), 10 nm/200 W (Ni), and 8 nm/500 W (TiW).

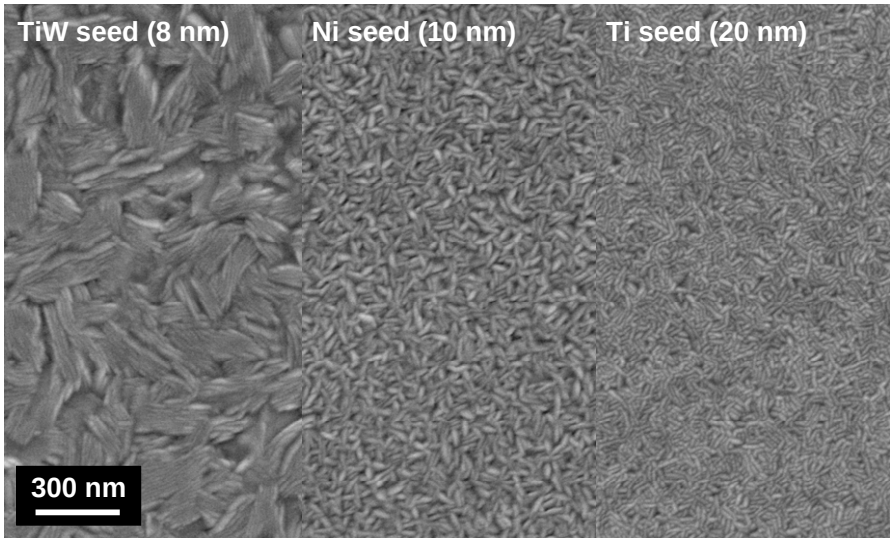

Figure 23. SEM images of the Mo surface morphology after deposition on thin TiW (8 nm), Ni (10 nm), and Ti (20 nm) seed layers [V].

The AFM RMS surface roughness of the Mo electrode is 0.4, 0.6, and 1.8 nm for Ti, Ni, and TiW, respectively. The Mo film consists of elongated grains whose size varies strongly with seed layer material. The largest grains are obtained with TiW, while small regular Mo grains grow on Ti films.

The various seed layers are expected to provide different crystalline templates for Mo electrode growth. Figure 24 shows θ-2θ XRD scans for the three optimized structures.

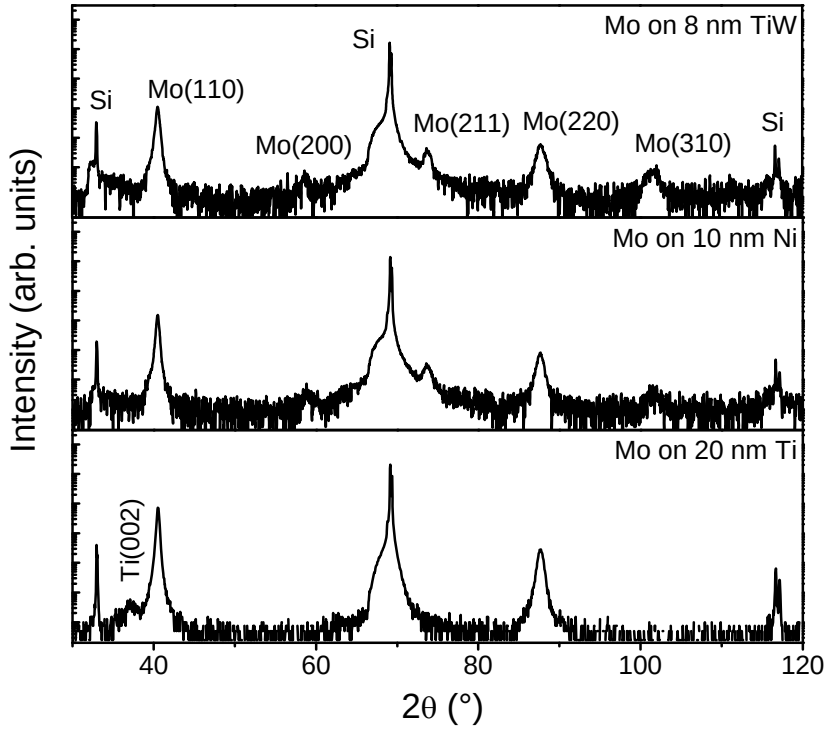

Figure 24. *θ-2θ* XRD scans of 300 nm thick Mo films on different seed layers [V].

The 300 nm thick Mo film is polycrystalline on top of all seed layers with a preferred (110) orientation. However, compared to Ni and TiW, the presence of other crystalline orientations is drastically reduced when the Mo film is grown onto Ti. The improved (110) orientation of the Mo film is also confirmed by the enhanced intensity and reduced width of the (110) reflection. The full width at half maximum (FWHM) of the Mo(110) peak is 0.30º, 0.33º, and 0.40º for Ti, Ni and TiW, respectively. With a smooth surface morphology and (110)-oriented film texture the Ti-seeded Mo electrodes provide the best template for high-quality AlN resonator films.

The AlN film properties were optimized by altering the deposition parameters including temperature, the N_2/Ar gas ratio, total sputter pressure, target power, DC-pulsing parameters, substrate bias, and base pressure. XRD measurements of the optimized AlN films grown onto Mo bottom electrodes with different seed layer materials are summarized in Fig. 25. The AlN grains are mainly (002) oriented. However, for Ni and in particular TiW seed layers, an additional AlN

(105) reflection is also measured, which is most likely related to the formation of some large misoriented clusters.

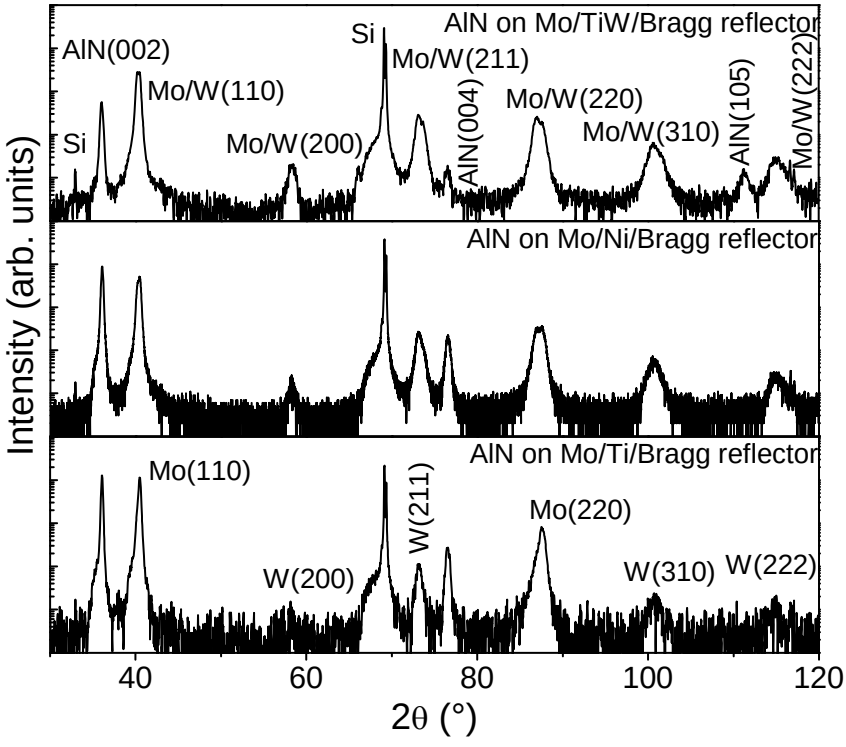

Figure 25. *θ-2θ* XRD scans of 1300 nm thick AlN films on top of a W/SiO_2 Bragg reflector and TiW-, Ni-, and Ti-seeded Mo electrodes [V].

The AlN film on top of the Ti/Mo layer shows the highest intensity of the (002) AlN peak indicating a high degree of texture along the c-axis. The FWHM of the (002) reflection of this film is only 0.21º, which compares well with the FWHM values of 0.24º and 0.31º for the AlN films on top of Ni/Mo and TiW/Mo. Also, the (002)-oriented grains are much better aligned along the substrate normal when the AlN film is grown onto Ti/Mo, as illustrated by the XRD rocking curves in Fig. 26.

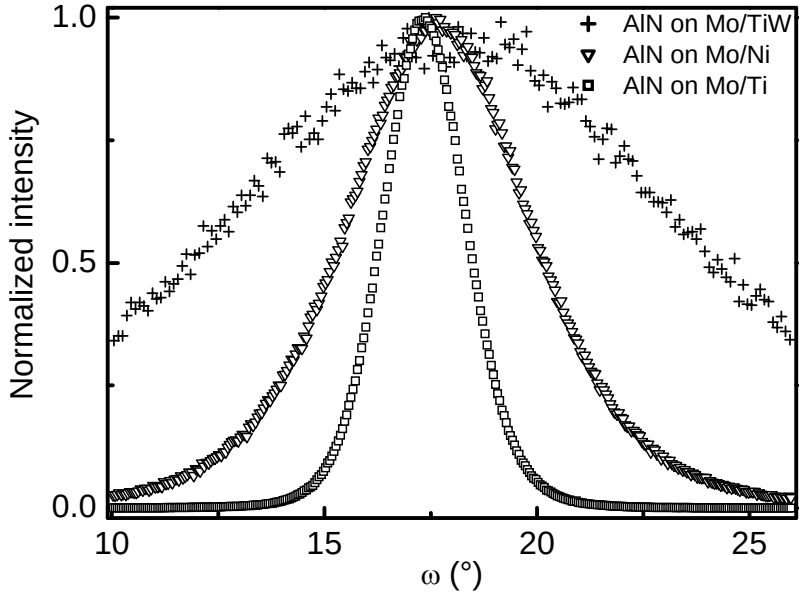

Fig. 26. XRD rocking curves of the AlN (002) reflection, normalized to the peak values. The maximum intensities were 530, 4600 and 16000 counts/s for AlN on TiW/Mo, Ni/Mo and Ti/Mo, respectively [V].

The FWHM of the rocking curves is 2.3º (Ti seed layer), 5.0º (Ni seed layer), and 12.3º (TiW seed layer). A strong correlation between the width of the rocking curve and the electro-acoustic coupling coefficient has previously been demonstrated and it has been shown that a FWHM of about 2° results in very good resonator performances [94]. However, optimization of the crystalline orientation and grain size is not sufficient. One other important factor is the density of 180° flipped grains [95]. These grains will neutralize the driving force of well-oriented grains and also affect the resonator *Q*-value.

Figure 27 shows a cross-sectional SEM picture of the fabricated AlN resonator with an optimized Mo bottom electrode deposited onto an acoustic SiO_2/W Bragg mirror.

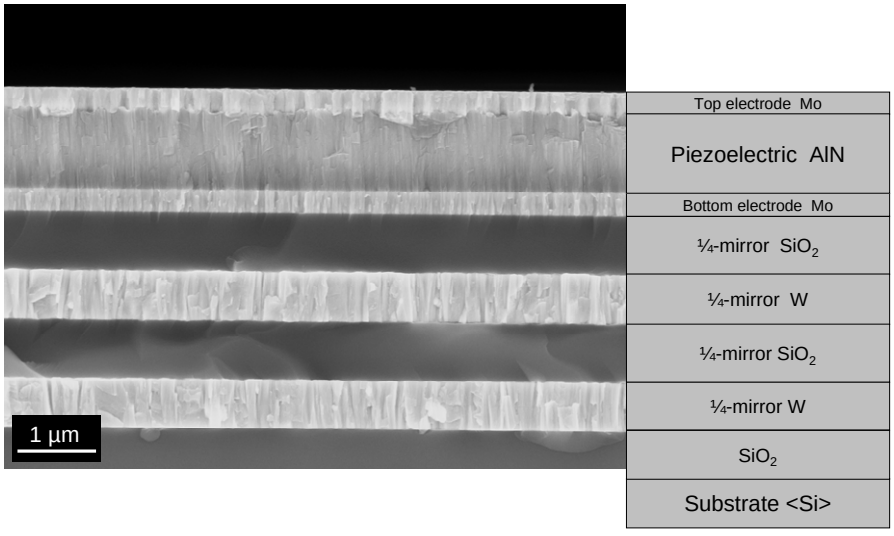

Figure 27. A cross-sectional SEM picture of the fabricated BAW resonator structure.

The surface roughness of the seed layer plays an important role in the quality of piezoelectric films. The smoother the seeding, the higher the quality of the AlN film is [85]. The surface finishing of the acoustic mirror with chemical mechanical polishing (CMP) is also crucial [96] to smooth the excess roughness caused by the W layers.

The measured S_{11} scattering parameter of 50 Ω resonators fabricated with TiW/Mo, Ni/Mo, and Ti/Mo bottom electrodes are displayed in Fig. 28.

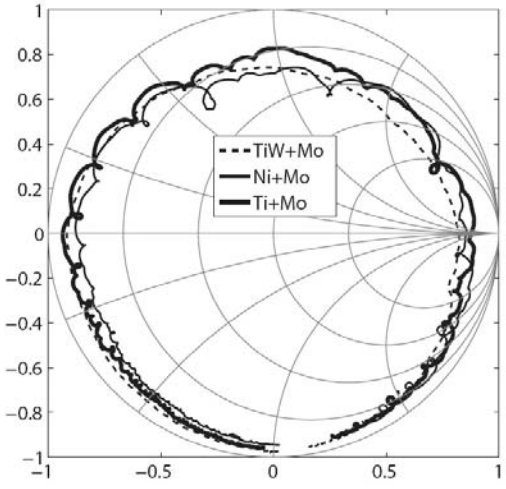

Figure 28. S_{11} scattering parameter of 50 Ω resonators displayed on a Smith chart [V].

The S_{11} values of the Ti/Mo-based resonator forms the largest circle in the Smith chart of Fig. 28, which corresponds to a large FoM of 80. The ripples are due to laterally standing plate wave resonances, which have not been suppressed in these resonators. The input impedances are shown in Fig. 29. To facilitate comparisons, the data is plotted against a frequency that is normalized by f_p and rescaled to match the f_p of the Ti/Mo-based resonator.

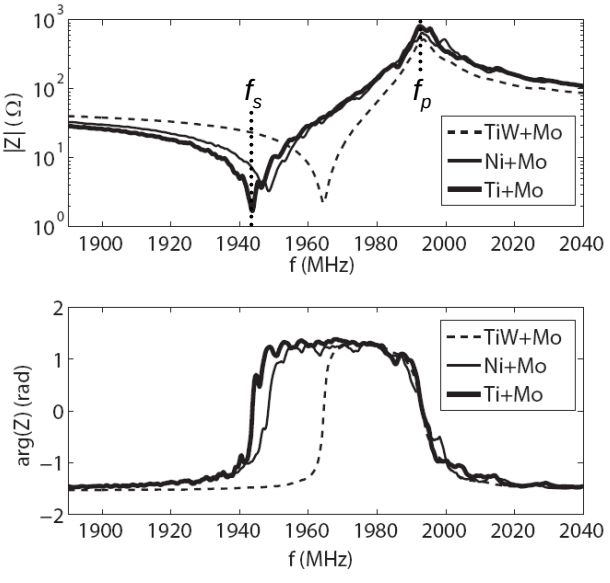

Figure 29. Impedance magnitude (upper plot) and phase of 50 Ω resonators [V].

The impedance plots clearly show that the electro-acoustic coupling coefficient K^2 drastically improves when the TiW/Mo bottom electrode is replaced by Ni/Mo as indicated by an increase of difference between f_p and f_s. A further improvement is obtained for Ti/Mo bottom electrodes. Whilst the electro-acoustic coupling coefficient of BAW resonators with Ti/Mo is already very good, further increases of K^2 are still anticipated upon a detailed optimization of the Mo electrode thickness [97]. The Q_{max}, K^2 and FoM values of the optimized Ti/Mo structure are 1276, 6.28 % and 80, respectively, for small area (50 Ω) devices. For large area devices (< 10 Ω), K^2 is 6.89 % but the slightly smaller Q-value of 1000 lowers the FoM to 69. The Q-values of the different resonator structures do not reveal any clear trends and the extracted values are somewhat prone to errors due to spurious ripples in the electro-acoustic response. Higher Q-values might be obtained by a re-design of the Bragg reflector [98]. The obtained electrical characteristics fulfill the requirements for RF device applications.

To further optimize the performance of BAW devices in the future, we tested the applicability of the layer transfer method to the fabrication of BAW resonators. The potential advantages of this method include decoupling of the electrode and seed layer functions. It thus offers total freedom to select a seed layer for optimal AlN growth. Moreover, as the both the bottom and top electrodes are deposited after the AlN film any kind of multilayer electrodes with optimal acoustic and electrical properties can be used. This method enables also the patterning of an acoustic mirror after AlN deposition.

AlN thin films were deposited onto a Si substrate with native oxide and the bottom Mo electrode and acoustic mirror consisting of SiO_2/W pairs were grown onto the AlN layer. A buffer layer of SiO_2 was subsequently deposited and CMP polished. Direct wafer bonding of the auxiliary wafer with the films to a device Si wafer was subsequently carried out. The auxiliary wafer was removed using mechanical grinding followed by plasma etching using an ICP etcher. Key aspect in the removal of the auxiliary substrate was the etch selectivity between Si and AlN. Finally, the top Mo electrode was deposited and patterned to form BAW resonators.

The Q_{max}, K^2, and FoM values of the devices obtained using the layer transfer method are 1060, 6.04 %, and 64, respectively, for small area (50 Ω) devices. The electrical properties of the transferred films are comparable to the values achieved by the conventional method. The small decrease in electrical response is potentially due to damages to the AlN surface which could be induced during plasma etching. This test, however, clearly demonstrated that the layer transfer

method can be used to fabricate BAW resonators without major deterioration of electrical properties. Consequently, the optimized piezoelectric response of the fabricated devices holds a great potential for RF resonator applications. As a next step we suggest the use of the layer transfer method in combination with innovative seed layers, multilayer electrodes, and acoustic mirrors. It is anticipated that this new fabrication method will lead BAW resonators with electro-acoustic responses that are beyond the current state-of-the-art.

7. Tantalum-based passive devices

The building elements of passive RF circuits include transmission lines, resistors, capacitors and inductors. Thin film fabrication techniques are very well suited for the fabrication of these components with the exception of inductors. In a planar assembly with an air core coil, the number of loops of an inductor remains inevitably small leading to low inductance. A low inductive reactance, ωL, results in low Q-values even if the ohmic losses R remain small (because $Q = \omega L/R$). This is the reason why inductors are not often used in thin film electronics. Thin film capacitors and resistors, on the other hand, are components that are widely used in RF circuits. For low-loss RF applications, capacitors and resistors must be integrated with highly conductive electrodes such as Cu.

In many thin film resistor designs, the resistive film is deposited prior to the electrodes and this facilitates the use of Cu as electrode material. Thin film resistors are commonly used in integrated circuits to bias active devices, serve as a voltage divider, and assist in impedance matching. The performance of thin film resistors is mainly defined by the sheet resistance and temperature coefficient of resistance (TCR). Moreover, the resistor should be highly stable at the operating conditions. On the other hand, the integration of highly conductive electrodes for fixed value thin film capacitors suffers the same problems as the BST capacitors described in Chapter 5. Capacitors at high frequencies find most use as isolators and impedance matching elements. The key factors are capacitance density (pF/mm^2) and Q-value. In order to make small devices, the capacitance density must be large. This requires a dielectric with high permittivity. Unfortunately high-permittivity dielectrics (usually oxides of heavy metals such as Ta, Hf, and Nb) have low Q-values. Here, control over the thin film deposition process becomes essential in tailoring the crucial material properties. Thin film growth techniques enable the fabrication of mixture compositions which can not be obtained in bulk crystal form. In this work, we focused on the development of tan-

talum pentoxide and tantalum nitride thin film processes for the fabrication of resistors and capacitors and the integration of highly conductive Cu electrodes.

The resistance of a resistor depends on the size (length and cross-sectional area) and resistivity of the material (composition) as depicted in Eq. 3. The operating temperature is also affecting the resistivity. Potential thin film resistor materials are polysilicon, silicon chrome (SiCr), nickel crome (NiCr) and tantalum-based materials.

Tantalum nitride is chemically inert, corrosion resistant, and hard, which makes it very attractive for use as structural elements in integrated circuits. For RF circuits, a precise resistance value, low TCR, and stability are required. The properties of TaN films depend strongly on the deposition conditions. The fabricated Ta_xN films with Cu electrodes were deposited by reactive RF magnetron sputtering. Figure 30 shows the influence of the nitrogen partial pressure on the deposition rate, film resistivity and crystalline phases.

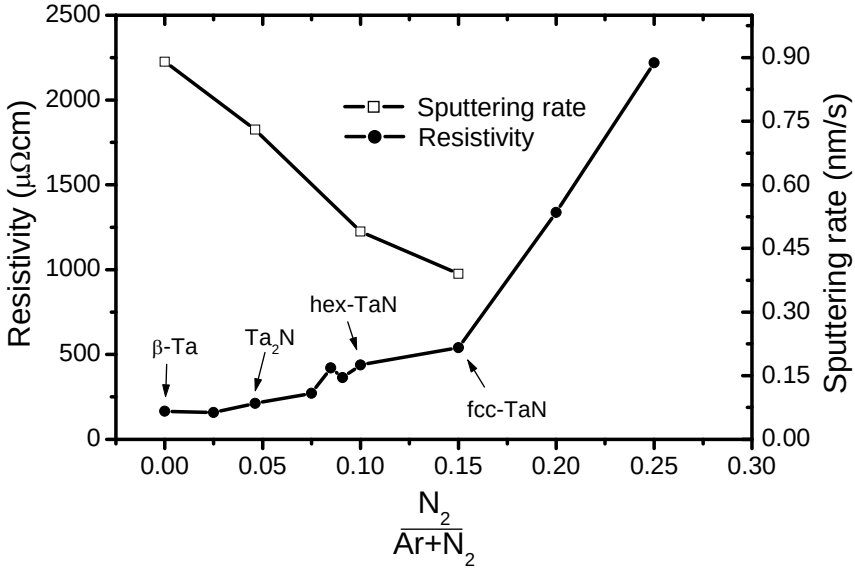

Figure 30. Resistivity and sputtering rate of Ta_xN films deposited at various N_2-Ar gas ratios. The crystalline phase as measured using XRD are also indicated in the figure [IV].

The sputtering rate reduces by 50 % when the nitrogen partial pressure is increased from 0 to 15 % due to target poisoning. Pure tantalum films can be grown with a body centered cubic (bcc) α-Ta phase or a tetragonal β-Ta phase [99]. The α-Ta phase exhibits a resistivity of 25 μΩcm, which is much less than

that of our films, and therefore we conclude that our films grow with a β-Ta phase in pure Ar atmosphere. By increasing the N_2 partial pressure from 5 % to 15 % we first obtained hexagonal Ta_2N, then a combination of hexagonal and cubic TaN, and finally pure cubic TaN. Nitrogen rich phases e.g. Ta_5N_6, Ta_4N_5 and Ta_3N_5 are formed after the fcc-TaN phase when the nitrogen partial pressure is further increased. The resistivities of these films are similar to those reported in literature [100, 101] and face centered cubic (fcc) TaN [102–104].

As precise resistivity measurements for resistors are required, thin film test resistors were used to determine the resistivity values across the wafer. The films were deposited onto thermally oxidized Si wafers. Figure 31 illustrates the resistivity values of Ta_xN films deposited at various N_2/Ar gas flow ratios measured from different locations on the 100 mm wafer. The on-wafer measurement was conducted using a four-point-probe technique.

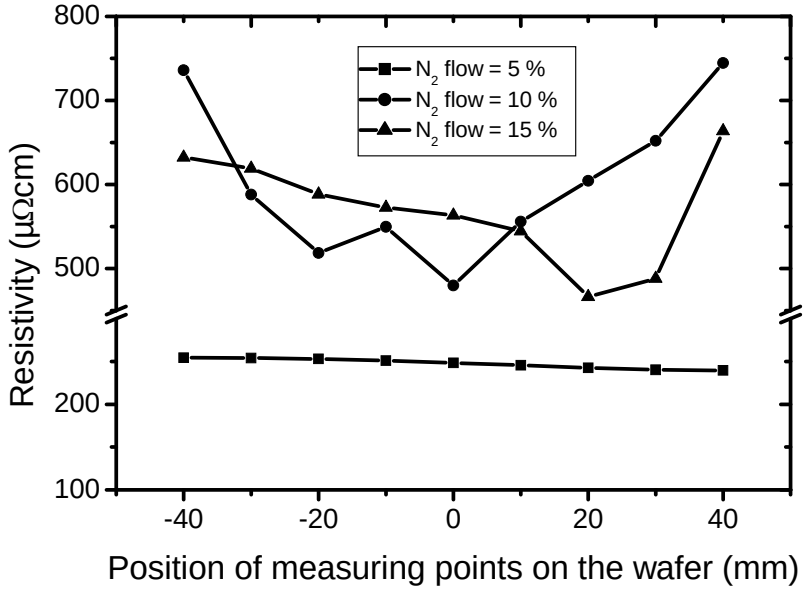

Figure 31. Variation in Ta_xN thin film resistivity across a 100 mm wafer for various N_2/Ar gas flow ratios during sputtering [IV].

Even though the films were uniform in thickness and the nitrogen content quantified by RBS varied slightly, the resistivity changes substantially for films deposited in 10 and 15 % N_2 partial gas pressure. The phase identified as Ta_2N, on the other hand, exhibits a constant resistivity value over a large composition

range. The Ta_2N phase is stable in a relatively wide nitrogen concentration range [46] and the process window is therefore wide. The TaN phase is only obtained for very specific N_2 partial pressure [46] and the process window is therefore narrow. In this case, the ratio of different phases changes across the wafer leading to resistivity variations in the films deposited at N_2 flow rates of more than 5 %. Thus only the Ta_2N phase obtained at 5 % N_2 partial gas flow is applicable for thin film resistor applications.

To fulfill tight tolerances for the resistors, the TCR value should be low. The temperature coefficient of resistance can be expressed as follows [100]:

$$TCR = \frac{R_1 - R_0}{R_0(T_1 - T_0)}, \tag{14}$$

where T_0 and R_0 are the room temperature and resistance at room temperature, and T_1 and R_1 are the temperature and resistivity at the measuring point. Figure 32 shows the temperature dependense of a Ta_2N resistor grown at 5 % N_2 partial gas flow. The Ta_2N test resistor had Cu electrodes.

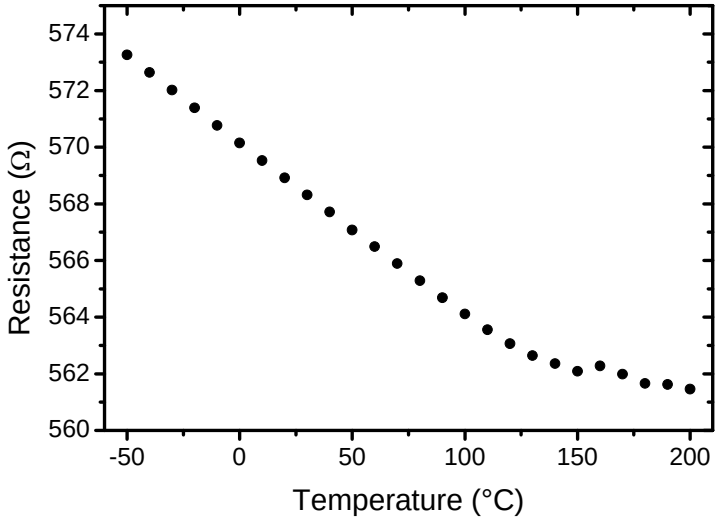

Figure 32. The variation of the resistance with temperature of a Ta_2N test resistor with Cu electrodes.

The negative slope indicates a semiconductor-like behavior and the linear resistance-temperature characteristics up to about 100 °C reflect a constant TCR

value os 103 ppm/°C for this device. The tantalum nitride (Ta_2N) thin film resistor exhibits reasonable stability and its high resistivity makes it suitable for integration into RF circuits.

In order to fabricate completely miniaturized RF circuits, a reduction of the capacitor size is essential. This can be achieved by using a high-dielectric constant material as an insulator. Fixed capacitors generally contain a metal/insulator/metal structure on an insulating substrate. The dielectric layer preferentially has a high dielectric constant and breakdown field strength, low leakage current characteristics, and a high *Q*-value. Tantalum pentoxide (Ta_2O_5) is a promising material to fulfill these requirements for integrated RF capacitor applications. Moreover, integration of tantalum pentoxide with highly conductive electrode materials such as Cu is essential for low device losses at high frequencies.

In our experiments the Ta_2O_5 thin films were reactively grown in an O_2/Ar atmosphere on a glass wafer using RF magnetron sputtering at room temperature. The successful integration of Cu bottom electrodes under these deposition conditions is troublesome as discussed in Chapter 3. The main problem relates to the oxidation of the Cu surface at relatively low temperatures [105]. To prevent this, we used a sacrificial Ta diffusion barrier between the Cu bottom electrode and the growing Ta_2O_5 film. Ta is known to be a good template for Ta_2O_5 crystallization [106] and it forms tantalum oxide in oxidizing atmosphere. Figure 33 shows a schematic cross-section picture of the MIM structure used.

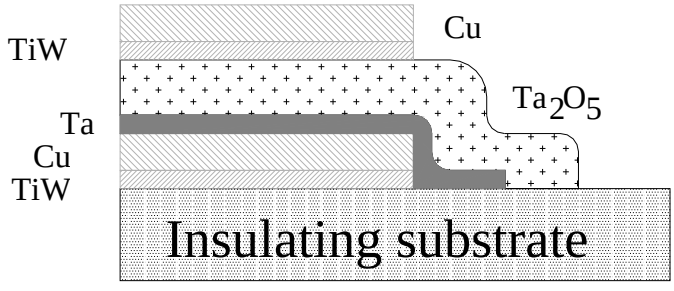

Figure 33. Schematic illustration of a Ta_2O_5 thin film capacitor equipped with a Ta diffusion barrier [III].

The sputtered tantalum pentoxide films crystallized into an orthorhombic β-Ta_2O_5 phase. RBS was used to determine the composition and stoichiometry of the films. Fully stoichiometric tantalum pentoxide films were obtained at a 20 % O_2/Ar gas flow ratio.

For actual device structures, the tantalum pentoxide films were deposited on patterned bottom Cu electrodes with a Ta diffusion barrier. Cu top electrodes were subsequently grown and patterned to form discrete MIM capacitors. The measured capacitors showed, irrespective of size, a relative dielectric permittivity (ε_r) of 25 which resembles values that have been previously reported [107]. For crystalline Ta_2O_5 values up to 40, and even 60 have been reported [107]. The capacitance density was high, 635 pF/mm^2 for a 340 nm thick dielectric layer, which is desirable for RF circuit miniaturization. Moreover, tantalum pentoxide films showed low leakage current properties: 2.0×10^{-6}, 3.9×10^{-6}, 5.7×10^{-6} A/cm^2 at the applied bias voltage of 5, 10, and 15 V.

The fabricated discrete capacitive structures exhibited a high *Q*-value of 650 at 100 kHz. However, a steep decrease of the *Q*-value at GHz frequencies was measured as illustrated Fig. 34. This reduction of the *Q*-value is predominantly due to parasitic inductance in the electrode leads and series resistance.

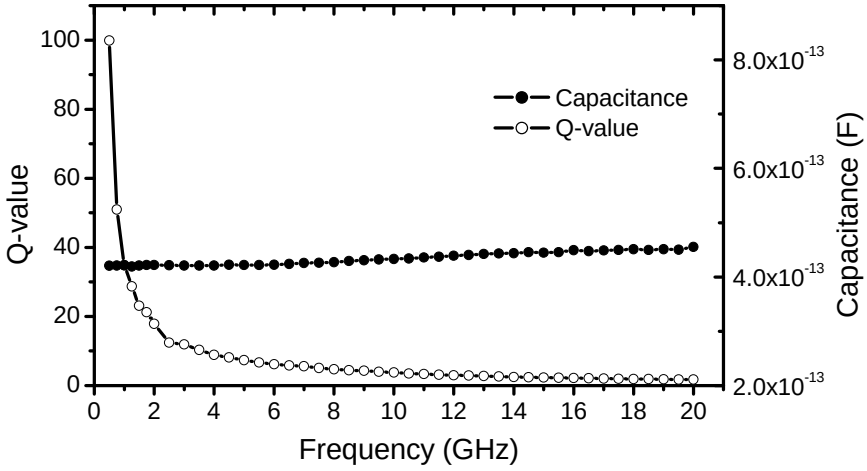

Figure 33. Q-value and capacitance versus frequency of a 30×30 μm^2 thin film tantalum pentoxide capacitor [III].

The Cu bottom and top electrodes of the fabricated capacitor structures were 245 and 500 nm thick. The decrease of the *Q*-value at high frequency might therefore be partly due to electrode losses as discussed in Chapters 3 and 5. A further increase of the electrode thickness can increase the *Q*-value at GHz frequencies. In spite of this, the capacitance of the fabricated structures is nearly constant over a frequency range up to 20 GHz. The fabricated Ta_2O_5 MIM capacitors thus hold a great promise for applications in miniaturized RF circuits.

8. Summary

The aim of this study was to develop and improve thin film fabrication techniques for multilayer RF microwave devices. The devices under study included tunable ferroelectric $Ba_xSr_{1-x}TiO_3$ (BST) and $Pb_xSr_{1-x}TiO_3$ (PST) parallel-plate capacitors, and piezoelectric AlN thin film bulk acoustic wave resonators. Furthermore, Ta_2O_5 and Ta_2N thin films were investigated for capacitor and resistor applications. To minimize electrode losses at GHz frequencies, highly conducting Cu and Mo electrode materials were integrated into these devices. The use of low-loss Cu electrodes was only possible after the development of a new layer transfer method for the fabrication of ferroelectric parallel-plate devices. This method was successfully used to structure polycrystalline BST and PST, and single crystalline $SrTiO_3$ (STO) tunable capacitors. The deposition of Mo electrodes was optimized on several seed layer materials and this resulted in ideal templates for high-quality AlN film. Moreover, AlN thin film BAW resonators were also fabricated using the layer transfer method. The fabricated device structures exhibited state-of-the-art dielectric and electro-acoustic properties and thus hold a great promise for practical RF applications.

This thesis comprises six refereed journal publications and the main results of these studies are summarized as follows:

In Publication I, we demonstrate that a new layer transfer method can be used for the fabrication of ferroelectric parallel-plate capacitors. By decoupling the seed layer and electrode functions, it was possible to use highly conductive Cu as the bottom electrode. First, a PST film was deposited by a sol-gel process onto a Pt seed layer. The layer transfer method was then used to fabricate tunable capacitors with a Cu/PST/Cu parallel-plate structure. The relative dielectric permittivity of the devices at room temperature was 420 and the tunability amounted to 73% near a breakdown voltage of 35 V. The use of Cu electrodes resulted in a giant electrode Q-factor×capacitor area product of $Q_{ele}A=3.79\times10^5$

μm^2 at 1 GHz. This clearly demonstrates the potential of the layer transfer method for the fabrication of ferroelectric parallel-plate capacitors with low-loss electrodes, which holds a great promise for microwave device applications.

Publication II describes problematic integration of highly conductive electrodes with ceramic thin films that are grown in a reactive atmosphere at high temperature. As the best conducting metals (Ag, Cu, Al) are not thermodynamically stable at these deposition conditions, the noble metals Au and Pt were examined as alternative electrode materials with a high oxidation resistance. In addition, growth and annealing experiments involving Mo electrodes with a sacrificial or thermally stable diffusion barrier were conducted. The electrode stacks were annealed at 650 °C in an open-end air furnace and in vacuum with a protective gas. The surface morphology, electrode cross-section, and film resistivity were measured to analyze the electrode stability. The experimental results indicate that the chemically inert materials (Au and Pt) failed to endure the high annealing temperature. Mo electrodes with a diffusion barrier were stable against oxidation, but their high resistivity will limit the device *Q*-value at GHz frequencies.

A sacrificial diffusion barrier concept is also adopted in Publication III to form discrete Ta_2O_5 MIM capacitors with Cu electrodes for high-frequency applications. In these experiments, the ceramic films were reactively sputtered in an Ar/O_2 atmosphere from a pure Ta deposition target onto β-Ta protected Cu electrodes. The oxygen partial pressure was controlled to tailor the film properties towards capacitor applications. Under optimized deposition conditions the films grew fully stoichiometric with an orthorhombic β-Ta_2O_5 phase onto the Ta diffusion barrier as illustrated by detailed XRD and RBS measurements. The devices exhibited low leakage characteristics, high capacitance density and a relative dielectric permittivity of 25. The device *Q*-value was 650 at 100 kHz and remained nearly constant up to 1 GHz.

In Publication IV we examine the fabrication of discrete Ta_xN thin film resistors using reactive magnetron sputtering. As the resistor design only requires top electrodes, the integration of highly conductive Cu was relatively straightforward. Detailed characterization of the Ta_xN film and resistor properties were conducted using XRD, RBS, AFM, and four-point probe measurements. A gradual change of the Ar/N_2 sputtering gas ratio resulted in different structural phases. Hexagonal Ta_2N grown in 5% N_2 turned out to be the most stable phase and the only one for which a constant resistivity could be obtained over a 100 mm wafer. The resistivity of the sputtered Ta_2N film was 234 μΩcm and its

temperature coefficient of resistance amounted -103 ppm/°C. These properties are suitable for resistors in integrated RF circuits.

The growth of high-quality AlN films by reactive pulsed-DC sputtering onto optimized Mo electrodes is studied in Publication V. In these experiments, we particularly focused on the influence of thin seed layers on the growth of the Mo bottom electrode and the piezoelectric AlN layer. The seed layer materials were TiW, Ni, and Ti. For optimal Mo film growth several deposition parameters, especially the thickness and sputtering power, of the seed layers were varied. Structural characterization of the films was performed using XRD, SEM, and AFM. Moreover, the electro-acoustic properties of complete BAW resonators were analyzed in detail around 2 GHz. The crystalline structure and morphology of the Mo and c-axis oriented AlN films were found to vary strongly with seed layer material and thickness. The smoothest Mo electrodes as well as most narrow AlN rocking curve were obtained for thin Ti seed layers. The performance of BAW resonators with a Ti-seeded Mo/AlN/Mo structure was very good, as indicated by a maximum electro-acoustic coupling constant of 6.89% and a quality factor of more than 1000.

In Publication VI we study the influence of substrate bias during RF magnetron sputtering of BST thin films onto platinized Si wafers. The crystalline structure, grain morphology, lattice strain and composition of the BST films were found to be significantly affected by the application of a substrate bias voltage. The main effects are due to a bias-induced change in the film composition at very high voltage and a gradual increase of the tensile in-plane film strain with substrate bias. These changes correlate with a significant increase of the relative dielectric permittivity and tunability at room temperature and, at very large substrate bias, a deterioration of the quality factor of Pt/BST/Pt parallel-plate capacitors. Based on our results, the performance of paraelectric and ferroelectric thin films can be improved by the application of a small to moderate substrate bias during growth. Tailoring of dielectric properties using substrate bias during magnetron sputtering opens a new route to the fabrication of tunable microwave devices.

References

1. Tiggelman, M.P.J., Reimann, K., Liu, J., Klee, M., Keur, W., Mauczock, R., Schmitz, J. & Hueting, R.J.E. Identifying dielectric and resistive electrode losses in high-density capacitors at radio frequencies. 2008 IEEE Conference on Microelectronic Test Structures, ICMTS, March 24, 2008 – March 27. 2008. Edinburgh, United Kingdom: Institute of Electrical and Electronics Engineers Inc, 2008. Pp. 190–195.

2. Lu, J. & Stemmer, S. Low-loss, tunable bismuth zinc niobate films deposited by rf magnetron sputtering. Applied Physics Letters, 2003. Vol. 83, No. 12, pp. 2411–2413.

3. Vorobiev, A., Rundqvist, P., Khamchane, K. & Gevorgian, S. Silicon substrate integrated high Q-factor parallel-plate ferroelectric varactors for microwave/millimeterwave applications. Applied Physics Letters, 2003. Vol. 83, No. 15, pp. 3144–3146.

4. Tombak, A., Maria, J., Ayguavives, F., Jin, Z., Stauf, G.T., Kingon, A.I. & Mortazawi, A. Tunable barium strontium titanate thin film capacitors for RF and microwave applications. IEEE Microwave and Wireless Components Letters, 2002. Vol. 12, No. 1, pp. 3–5.

5. Acikel, B., Taylor, T.R., Hansen, P.J., Speck, J.S. & York, R.A. A new high performance phase shifter using $Ba_xSr_{1-X}TiO_3$ thin films. IEEE Microwave and Wireless Components Letters, 2002. Vol. 12, No. 7, pp. 237–239.

6. Dube, D.C., Baborowski, J., Muralt, P. & Setter, N. The effect of bottom electrode on the performance of thin film based capacitors in the gigahertz region. Applied Physics Letters, 1999. Vol. 74, No. 23, pp. 3546–3548.

7. Dimos, D. & Mueller, C.H. Perovskite thin films for high-frequency capacitor applications. Annual Review of Materials Science, 1998. Vol. 28, pp. 397–419.

8. Bao, P., Jackson, T.J., Wang, X. & Lancaster, M.J. Barium strontium titanate thin film varactors for room-temperature microwave device applications. Journal of Physics D: Applied Physics, 2008. Vol. 41, 063001 (21 pp.)

9. Setter, N., Damjanovic, D., Eng, L., Fox, G., Gevorgian, S., Hong, S., Kingon, A., Kohlstedt, H., Park, N.Y., Stephenson, G.B., Stolitchnov, I., Taganstev, A.K., Taylor, D.V., Yamada, T. & Streiffer, S. Ferroelectric thin films: review of materials, properties, and applications. Journal of Applied Physics, 2006. Vol. 100, No. 5, pp. 51606–1–46.

10. Fu, X., Shan, L., Ding, B., Hou, W., Fang, Z. & Fu, Z. Progress of (Sr, Ba) TiO_3 ferroelectric thin film and tunability. Bulletin of Materials Science, 2004. Vol. 27, No. 5, pp. 433–439.

11. Zhu, X., Zhu, J., Zhou, S., Liu, Z., Ming, N., Lu, S., Chan, H.L. & Choy, C. Recent progress of (Ba,Sr)TiO_3 thin films for tunable microwave devices. Journal of Electronic Materials, 2003. Vol. 32, No. 10, pp. 1125–1134.

12. Tagantsev, A.K., Sherman, V.O., Astafiev, K.F., Venkatesh, J. & Setter, N. Ferroelectric materials for microwave tunable applications. Journal of Electroceramics, 2003. Vol. 11, No. 1–2, pp. 5–66.

13. Xi, X.X., Li, H., Si, W., Sirenko, A.A., Akimov, I.A., Fox, J.R., Clark, A.M. & Hao, J. Oxide thin films for tunable microwave devices. Journal of Electroceramics, 2000. Vol. 4, No. 2, pp. 393–405.

14. Vendik, O.G., Hollmann, E.K., Kozyrev, A.B. & Prudan, A.M. Ferroelectric tuning of planar and bulk microwave devices. Journal of Superconductivity, 1999. Vol. 12, No. 2, pp. 325–338.

15. Lancaster, M.J., Powell, J. & Porch, A. Thin-film ferroelectric microwave devices. Superconductor Science and Technology, 1998. Vol. 11, No. 11, pp. 1323–1334.

16. Padmini, P., Taylor, T.R., Lefevre, M.J., Nagra, A.S., York, R.A. & Speck, J.S. Realization of high tunability barium strontium titanate thin films by rf magnetron sputtering. Applied Physics Letters, 1999. Vol. 75, No. 20, pp. 3186–3188.

17. Im, J., Auciello, O., Baumann, P.K., Streiffer, S.K., Kaufman, D.Y. & Krauss, A.R. Composition-control of magnetron-sputter-deposited $(Ba_xSr_{1-x})Ti_{1+y}O_{3+z}$ thin films for voltage tunable devices. Applied Physics Letters, 2000. Vol. 76, No. 5, pp. 625–627.

18. Ayguavives, T., Tombak, A., Maria, J., Stauf, G.T., Ragaglia, C., Roeder, J., Mortazawi, A. & Kingon, A.I. Physical properties of (Ba,Sr)TiO_3 thin films used for integrated capacitors in microwave applications. Proceedings of the 2000 12th IEEE International Symposium on Applications of Ferroelectrics. 21 July–2 Aug. 2000. Vol. 1. Piscataway, NJ, USA: IEEE, 2001. ISAF 2000. Pp. 365–368.

19. Pervez, N.K., Hansen, P.J. & York, R.A. High tunability barium strontium titanate thin films for rf circuit applications. Applied Physics Letters, 2004. Vol. 85, No. 19, pp. 4451–4453.

20. Basceri, C., Streiffer, S.K., Kingon, A.I. & Waser, R. Dielectric response as a function of temperature and film thickness of fiber-textured (Ba,Sr)TiO_3 thin films

grown by chemical vapor deposition. Journal of Applied Physics, 1997. Vol. 82, No. 5, pp. 2497–2504.

21. Lakin, K.M., Kline, G.R. & McCarron, K.T. Development of miniature filters for wireless applications. Part 1 (of 3), May 16, 1995 – May 20. 1995. Vol. 2. Orlando, FL, USA: IEEE, 1995. Proceedings of the 1995 IEEE MTT-S International Microwave Symposium. Pp. 883–886.

22. Aigner, R. Bringing BAW Technology into Volume Production: The Ten Commandments and the Seven Deadly Sins. Proceedings of the Third International Symposium on Acoustic Wave Devices for Future Mobile Communication Systems. Chiba, Japan, March. 2007.

23. Mahon, S. & Aigner, R. Bulk acoustic wave devices – Why, how, and where they are going. CS MANTECH Conference. Austin, Texas, USA, May 14–17. 2007. Pp. 15–18.

24. Fattinger, G., Aigner, R. & Marksteiner, S. Everything you always wanted to know about BAW. Workshop proceedings APMC2006. Yokohama, Dec. 2006.

25. Satoh, Y., Nishihara, T., Yokoyama, T., Ueda, M. & Miyashita, T. Development of piezoelectric thin film resonator and its impact on future wireless communication systems. Japanese Journal of Applied Physics, Part 1: Regular Papers and Short Notes and Review Papers, 2005. Vol. 44, No. 5, pp. 2883–2894.

26. Jansman, A.B.M., Vanhelmont, F., Milsom, R.F., Ruigrok, J., De Bruijn, F., Lufting, R. & Lobeek, J.W. Bulk acoustic wave resonators and filters 2D modelling and industrialization aspects. 2005 IEEE Ultrasonics Symposium, September 18,2005 – September 21. 2005. Vol. 1. Rotterdam, Netherlands: Institute of Electrical and Electronics Engineers Inc, 2005. Pp. 97–100.

27. Lanz, R. & Lambert, C. Volume manufacturing aspects of BAW filters on a production cluster system. 2005 IEEE Ultrasonics Symposium, September 18,2005 - September 21. 2005. Vol. 1. Rotterdam, Netherlands: Institute of Electrical and Electronics Engineers Inc, 2005. Pp. 210–214.

28. Rubi, R. FBAR – from technology development to production. Proceedings of the second International Symposium on Acoustic Wave Devices for Future Mobile Communication Systems. Chiba University, Japan, March 3–5. 2004.

29. Lambert, C., Borrello, D., Choffat, H., Jacot, P. & Kuegler, E. BAW devices: Technology overview and manufacturing aspects. Proceedings of the second International Symposium on Acoustic Wave Devices for Future Mobile Communication System. Chiba university, Japan, March 3–5. 2004.

30. Aigner, R. Volume manufacturing of BAW-filters in a CMOS fab. Proceedings of the second International Symposium on Acoustic Wave Devices for Future Mobile Communication Systems. Chiba University, Japan, March 3–5. 2004.

31. Lakin, K.M. A review of thin-film resonator technology. IEEE Microwave Magazine, 2003. Vol. 4, No. 4, pp. 61–67.

32. Dubois, M.-A. Thin Film Bulk Acoustic Wave Resonators: A Technology Overview. MEMSWAVE 03. Toulous, France, July 2–4. 2003.

33. Michaelson, H. The work function of the elements and its periodicity. Journal of Applied Physics,1977. Vol. 48, No. 11, pp. 4729–4733.

34. Pervez, N.K. & York, R.A. Geometry-dependent quality factors in $Ba_{0.5}Sr_{0.5}TiO_3$ parallel-plate capacitors. IEEE Transactions on Microwave Theory and Techniques, 2007. Vol. 55, No. 2, pp. 410–417.

35. Lu, J., Schmidt, S., Boesch, D.S., Pervez, N., York, R.A. & Stemmer, S. Low-loss tunable capacitors fabricated directly on gold bottom electrodes. Applied Physics Letters, 2006. Vol. 88, 112905-1–3.

36. Park, J., Lu, J., Stemmer, S. & York, R.A. Microwave dielectric properties of tunable capacitors employing bismuth zinc niobate thin films. Journal of Applied Physics, 2005. Vol. 97, 084110-1–4.

37. Acikel, B. High Performance Barium Strontium Titanate Varactor Technology for Low Cost Circuit Applications. PhD Thesis, University of California Santa Barbara, 2002.

38. Hwang, L. & Turlik, I. A review of the skin effect as applied to thin film interconnections. IEEE transactions on components, hybrids, and manufacturing technology, 1992. Vol. 15, No. 1, pp. 43–55.

39. Rossnagel, S.M. & Kuan, T.S. Alteration of Cu conductivity in the size effect regime. Journal of Vacuum Science & Technology B, 2004. Vol. 22, No. 1, pp. 240–247.

40. Franssila, S., Kattelus, H. & Nykanen, E. Reduction of molybdenum resistivity by a seed layer of Ti-W. Microelectronic Engineering, 1997. Vol. 37–38, pp. 373–380.

41. Ezhilvalavan, S. & Tseng, T. Progress in the developments of $(Ba,Sr)TiO_3$ (BST) thin films for Gigabit era DRAMs. Materials Chemistry and Physics, 2000. Vol. 65, No. 3, pp. 227–248.

42. Tsai, M.S., Sun, S.C. & Tseng, T. Effect of bottom electrode materials on the electrical and reliability characteristics of (Ba, Sr)TiO_3 capacitors. IEEE Transactions on Electron Devices, 1999. Vol. 46, No. 9, pp. 1829–1838.

43. Fan, W., Kabius, B., Miller, J.M., Saha, S., Carlisle, J.A., Auciello, O., Chang, R.P.H. & Ramesh, R. Materials science and integration bases for fabrication of $(Ba_xSr_{1-x})TiO_3$ thin film capacitors with layered Cu-based electrodes. Journal of Applied Physics, 2003. Vol. 94, No. 9, pp. 6192–6200.

44. Stauf, G.T., Ragaglia, C., Roeder, J.F., Vestyck, D., Maria, J.P., Ayguavives, T., Kingon, A., Mortazawi, A. & Tombak, A. Thick electrodes for high frequency high Q tunable ferroelectric thin film varactors. Thirteenth International Symposium on Integrated Ferroelectrics. 11–14 March 2001. Vol. 39. Netherlands: Gordon & Breach, 2001. Pp. 321–330.

45. Maria, J., Boyette, B., Kingon, A., Ragaglia, C. & Stauf, G. Low loss tungsten-based electrode technology for microwave frequency BST varactors. Journal of Electroceramics, 2005. Vol. 14, No. 1, pp. 75–81.

46. Massalski, T.B. Binary Alloy Phase Diagrams. ASM International, 1996.

47. Nam, H., Choi, D. & Lee, W. Formation of hillocks in Pt/Ti electrodes and their effects on short phenomena of PZT films deposited by reactive sputtering. Thin Solid Films, 2000. Vol. 371, No. 1, pp. 264–271.

48. Olowolafe, J.O., Jones, R.E., Campbell, A.C., Hegde, R.I., Mogab, C.J. & Gregory, R.B. Effects of anneal ambients and Pt thickness on Pt/Ti and Pt/Ti/TiN interfacial reactions. Journal of Applied Physics, 1993. Vol. 73, No. 4, pp. 1764–1764.

49. Matsui, Y., Suga, M., Hiratani, M., Miki, H. & Fujisaki, Y. Oxygen diffusion in Pt bottom electrodes of ferroelectric capacitors. Japanese Journal of Applied Physics, Part 2: Letters, 1997. Vol. 36, No. 9A/B, pp. L1239–L1241.

50. Jae-Chang Lee & Soon-Gil Yoon. Characterization of $(Ba_{1-x},Sr_x)TiO_3$ thin films deposited on Pt/Ti/SiO_2/Si substrates with different Ti buffer layer thicknesses. Journal of Vacuum Science & Technology B, 1999. Vol. 17, No. 5, pp. 2182–2185.

51. Johnson, J.A., Lisoni, J.G. & Wouters, D.J. Developing a conductive oxygen barrier for ferroelectric integration. Microelectronic Engineering, 2003. Vol. 70, pp. 377–383.

52. Song, Z., Chong, N., Wong Chan, L.H., Choy, C. & Lin, C. Thermal stability of electrode stacks for application in oxide film devices. Thin Solid Films, 2002. Vol. 406, No. 1–2, pp. 268–274.

53. Maeder, T., Sagalowicz, L. & Muralt, P. Stabilized platinum electrodes for ferroelectric film deposition using Ti, Ta and Zr adhesion layers. Japanese Journal of Applied Physics, Part 1,1998. Vol. 37, No. 4, pp. 2007–2012.

54. Chinmulgund, M., Inturi, R.B. & Barnard, J.A. Effect of Ar gas pressure on growth, structure, and mechanical properties of sputtered Ti, Al, TiAl, and Ti_3Al films. Thin Solid Films, 1995. Vol. 270, pp. 260–263.

55. Rundqvist, P., Liljenfors, T., Vorobiev, A., Olsson, E. & Gevorgian, S. The effect of SiO_2, Pt, and Pt/Au templates on the microstructure and permittivity of $Ba_xSr_{1-x}TiO_3$ films. Journal of Applied Physics, 2006. Vol. 100, 114116-1-9.

56. Streiffer, S.K., Basceri, C., Parker, C.B., Lash, S.E. & Kingon, A.I. Ferroelectricity in thin films: The dielectric response of fiber-textured $(Ba_xSr_{1-x})Ti_{1+y}O_{3+z}$ thin films grown by chemical vapor deposition. Journal of Applied Physics, 1999. Vol. 86, No. 8, pp. 4565–4575.

57. Suni, T. Direct wafer bonding for MEMS and microelectronics. PhD Thesis, Helsinki University of Technology, 2006.

58. Niklaus, F., Stemme, G., Lu, J.Q. & Gutmann, R.J. Adhesive wafer bonding. Journal of Applied Physics, 2006. Vol. 99, 031101-1-28.

59. Taklo, M.M.V., Storås, P., Schjlberg-Henriksen, K., Hasting, H.K. & Jakobsen, H. Strong, high-yield and low-temperature thermocompression silicon wafer-level bonding with gold. Journal of Micromechanics and Microengineering, 2004. Vol. 14, No. 7, pp. 884–890.

60. Park, Y., Ruglovsky, J.L., Dicken, M.J. & Atwater, H.A. Bulk-like ferroelectric and piezoeletric properties of transferred-$BaTiO_3$ single crystal thin films. Materials Research Society Symposium Proceedings, April 13,2004 – April 16. 2004. San Francisco, CA, United states, 2004. Vol. 811, pp. E231–E236.

61. Lee, Y.S., Djukic, D., Roth, R.M., Laibowitz, R., Izuhara, T., Osgood Jr., R.M., Bakhru, S., Bakhru, H., Si, W. & Welch, D. Fabrication of patterned single-crystal $SrTiO_3$ thin films by ion slicing and anodic bonding. Applied Physics Letters, 2006. Vol. 89, 122902-1-3.

62. Ruglovsky, J.L., Park, Y., Ryan, C.A. & Atwater, H.A. Wafer bonding and layer transfer for thin film ferroelectrics. Materials Research Society Symposium Pro-

ceedings, December 02, 2002 – December 05. 2002. Boston, MA, United States, 2003. Vol. 748, pp. U1171–U1176.

63. Haisma, J., Spierings, B.A.C.M., Biermann, U.K.P. & van Gorkum, A.A. Diversity and feasibility of direct bonding: a survey of a dedicated optical technology. Applied Optics, 1994. Vol. 33, No. 7, pp. 1154–1169.

64. Alexe, M., Kaestner, G., Hesse, D. & Goesele, U. Ferroelectric-semiconductor heterostructures obtained by direct wafer bonding. Applied Physics Letters, 1997. Vol. 70, No. 25, pp. 3416–3418.

65. Akdogan, E.K., Bellotti, J. & Safari, A. Extrinsic loss mechanisms in BST for tunable RF/microwave passive components. 12th IEEE International Symposium on Applications of Ferroelectrics, July 21, 2000 – August 02. 2000. Honolulu, HI, United states: Institute of Electrical and Electronics Engineers Inc, 2000. Vol. 1, pp. 191–194.

66. Shaw, T.M., Suo, Z., Huang, M., Liniger, E., Laibowitz, R.B. & Baniecki, J.D. Effect of stress on the dielectric properties of barium strontium titanate thin films. Applied Physics Letters, 1999. Vol. 75, No. 14, pp. 2129–2131.

67. Gevorgian, S.S. & Kollberg, E.L. Do we really need ferroelectrics in paraelectric phase only in electrically controlled microwave devices? IEEE Transactions on Microwave Theory and Techniques, 2001. Vol. 49, No. 11, pp. 2117–2124.

68. York, R., Nagra, A., Erker, E., Taylor, T., Periaswamy, P., Speck, J., Streiffer, S. & Auciello, O. Microwave integrated circuits using thin-film BST. 12th IEEE International Symposium on Applications of Ferroelectrics, July 21, 2000 – August 02. 2000. Honolulu, HI, United states: Institute of Electrical and Electronics Engineers Inc, 2000. Vol. 1, pp. 195–200.

69. Lee, W., Park, I., Jang, G. & Kim, H. Electrical properties and crystal structure of $(Ba_{0.5}Sr_{0.5})TiO_3$ thin films prepared on $Pt/SiO_2/Si$ by RF magnetron sputtering. Japanese Journal of Applied Physics, Part 1, 1995. Vol. 34, No. 1, pp. 196–199.

70. Hong, S., Bak, H., An, I. & Ok, K.K. Microstructural and electrical properties of $Ba_xSr_{1-x}TiO_3$ thin films on various electrodes. Japanese Journal of Applied Physics, Part 1, 2000. Vol. 39, No. 4, pp. 1796–1800.

71. Zhu, X., Zheng, D., Peng, W., Zhu, J., Yuan, X., Li, J., Zhang, M., Chen, Y., Tian, H. & Xu, X. Preparation, microstructure and dielectric properties of $Ba_{0.5}Sr_{0.5}TiO_3$ thin films grown on $Pt/Ti/SiO_2/Si$ substrates by pulsed laser deposition. Materials Letters, 2004. Vol. 58, No. 27–28, pp. 3591–3596.

72. Li, S., Yang, Y.Q., Liu, L., Zhang, T.J. & Huang, W.H. Influence of deposition parameters on preferred orientation of RF magnetron sputtered BST thin films. Journal of Materials Science: Materials in Electronics, 2008. Vol. 19, No. 3, pp. 223–226.

73. Auciello, O., Saha, S., Kaufman, D.Y., Streiffer, S.K., Fan, W., Kabius, B., Im, J. & Baumann, P. Science and technology of high dielectric constant thin films and materials integration for application to high frequency devices. Journal of Electroceramics, 2004. Vol. 12, No. 1–2, pp. 119–131.

74. Nguyen, M., Yan, W.D. & Horne, E.P.W. Broadband tunable filters using high Q passive tunable ICs. 2008 IEEE MTT-S International Microwave Symposium Digest, MTT, June 15, 2008 – June 20. 2008. Atlanta, GA, United states: Institute of Electrical and Electronics Engineers Inc, 2008. Pp. 951–954.

75. Vendik, O.G. & Zubko, S.P. Ferroelectric phase transition and maximum dielectric permittivity of displacement type ferroelectrics ($Ba_xSr_{1-x}TiO_3$). Journal of Applied Physics, 2000. Vol. 88, No. 9, pp. 5343–5350.

76. Taylor, T.R., Hansen, P.J., Acikel, B., Pervez, N., York, R.A., Streiffer, S.K. & Speck, J.S. Impact of thermal strain on the dielectric constant of sputtered barium strontium titanate thin films. Applied Physics Letters, 2002. Vol. 80, No. 11, pp. 1978–1980.

77. Lakin, K.M. Thin film resonators and filters. 1999 IEEE Ultrasonics Symposium Proceedings. 17–20 Oct. NJ, USA: Institute of Electrical and Electronics Engineers Inc, 1999. Vol. 2, pp. 895–906.

78. Aigner, R. MEMS in RF-filter applications: Thin film bulk-acoustic-wave technology. 13th International Conference on Solid-State Sensors and Actuators and Microsystems, TRANSDUCERS '05, June 05, 2005 – June 09. 2005. Seoul, Republic of Korea: Institute of Electrical and Electronics Engineers Computer Society, 2005. Vol. 1, pp. 175–210.

79. Lobeek, J. & Smolders, A.B. Design and industrialisation of solidly-mounted BAW filters. 2006 IEEE MTT-S International Microwave Symposium Digest, June 11, 2006 – June 16. 2006. San Francisco, CA, United states: Institute of Electrical and Electronics Engineers Inc, 2006. Pp. 386–389.

80. Lanz, R., Senn, L., Gabathuler, L., Huiskamp, W., Strijbos, R.C. & Vanhelmont, F. Uniformity optimization of the electromechanical coupling coefficient in AlN based bulk acoustic wave resonators. 2007 IEEE Ultrasonics Symposium, IUS, October 28, 2007 – October 31. 2007. New York, NY, United states: Institute of Electrical and Electronics Engineers Inc, 2007. Pp. 1429–1432.

81. Naik, R.S., Reif, R., Lutsky, J.J. & Sodini, C.G. Low-temperature deposition of highly textured aluminum nitride by direct current magnetron sputtering for applications in thin-film resonators. Journal of the Electrochemical Society, 1999. Vol. 146, No. 2, pp. 691–696.

82. Iriarte, G.F., Bjurström, J., Westlinder, J., Engelmark, F. & Katardjiev, I.V. Synthesis of C-axis-oriented AlN thin films on high-conducting layers: Al, Mo, Ti, TiN, and Ni. IEEE transactions on ultrasonics, ferroelectrics, and frequency control, 2005. Vol. 52, No. 7, pp. 1170–1174.

83. Ohara, R., Sano, K., Yanase, N., Yasumoto, T., Kawakubo, T. & Itaya, K. High-Q thin film bulk acoustic wave resonator using highly <111> oriented aluminum electrode. 2005 IEEE Ultrasonics Symposium, September 18, 2005 – September 21. 2005. Rotterdam, Netherlands: Institute of Electrical and Electronics Engineers Inc, 2005. Vol. 1, pp. 206–209.

84. Lee, J., Jung, J., Lee, M. & Park, J. Effects of bottom electrodes on the orientation of AlN films and the frequency responses of resonators in AlN-based FBARs. Thin Solid Films, 2004. Vol. 447–448, pp. 610–614.

85. Lee, S., Lee, J. & Yoon, K.H. Growth of highly c-axis textured AlN films on Mo electrodes for film bulk acoustic wave resonators. Journal of Vacuum Science and Technology A: Vacuum, Surfaces and Films, 2003. Vol. 21, No. 1, pp. 1–5.

86. Dubois, M.A. & Muralt, P. Stress and piezoelectric properties of aluminum nitride thin films deposited onto metal electrodes by pulsed direct current reactive sputtering. Journal of Applied Physics, 2001. Vol. 89, No. 11, pp. 6389–6389.

87. Martin, F., Muralt, P. & Dubois, M. Process optimization for the sputter deposition of molybdenum thin films as electrode for AlN thin films. Journal of Vacuum Science and Technology A: Vacuum, Surfaces and Films, 2006. Vol. 24, No. 4, pp. 946–952.

88. Kamohara, T., Akiyama, M., Ueno, N., Nonaka, K. & Tateyama, H. Growth of highly c-axis-oriented aluminum nitride thin films on molybdenum electrodes using aluminum nitride interlayers. Journal of Crystal Growth, 2005. Vol. 275, No. 3–4, pp. 383–388.

89. Akiyama, M., Ueno, N., Tateyama, H., Nagao, K. & Yamada, T. Preparation of highly oriented aluminum nitride thin films on molybdenum bottom electrodes using metal interlayers. Journal of Materials Science, 2005. Vol. 40, No. 5, pp. 1159–1162.

90. Matsumoto, H., Asai, K., Kobayashi, N., Nagashima, S., Isobe, A., Shibagaki, N. & Hikita, M. Influence of underlayer materials on preferred orientations of sput-

ter-deposited AlN/Mo bilayers for film bulk acoustic wave resonators. Japanese Journal of Applied Physics, Part 1, 2004. Vol. 43, No. 12, pp. 8219–8222.

91. Lee, H.C, Park, J.Y., Lee K.H. & Bu J.U. Preparation of highly textured Mo and AlN films using a Ti seed layer for integrated high-Q film bulk acoustic resonators. Journal of Vacuum Science & Technology B, 2004. Vol. 22, No. 3, pp. 1127–1133.

92. Lee, S.-H., Kang, S.C., Han, S.C., Ju, B.K., Yoon, K.H. & Lee, J.-K. Role of AlN Piezoelectric Crystal Orientation in Solidly Mounted Film Bulk Acoustic Wave Resonators. Journal of the Korean Ceramic Society, 2003. Vol. 40, No. 4, pp. 393–397.

93. Kyung, H.Y., Kim, S.K., Chalapathy, R.B.V., Yun, J.H., Jeong, C.L., Song, J. & Byung, T.A. Characterization of a molybdenum electrode deposited by sputtering its effect on Cu(In,Ga)Se_2 solar cells. Journal of the Korean Physical Society, 2004. Vol. 45, No. 4, pp. 1114–1118.

94. Loebl, H.P., Klee, M., Metzmacher, C., Brand, W., Milsom, R. & Lok, P. Piezoelectric thin AlN films for bulk acoustic wave (BAW) resonators. Materials Chemistry and Physics, 2003. Vol. 79, No. 2–3, pp. 143–146.

95. Ruffner, J.A., Clem, P.G., Tuttle, B.A., Dimos, D. & Gonzales, D.M. Effect of substrate composition on the piezoelectric response of reactively sputtered AlN thin films. Thin Solid Films, 1999. Vol. 354, No. 1, pp. 256–261.

96. Molarius, J., Kulawski, M., Pensala, T. & Ylilammi, M. New Approach to Improve the Piezoelectric Quality of ZnO Resonator Devices by Chemomechanical Polishing. In: Fecht, H. & Werner, M. The Nano-Micro Interface: Bringing the Micro and Nano Worlds Together. (Wiley-VCH Weinheim), 2004. Pp. 181–193.

97. Lakin, K.M., Belsick, J., McDonald, J.F. & McCarron, K.T. Improved bulk wave resonator coupling coefficient for wide bandwidth filters. 2001 Ultrasonics Symposium, October 06,2001 - October 10. 2001. Vol. 1. Atlanta, GA, United states: Institute of Electrical and Electronics Engineers Inc, 2001. Pp. 827–831.

98. Marksteiner, S., Kaitila, J., Fattinger, G.G. & Aigner, R. Optimization of acoustic mirrors for solidly mounted BAW resonators. 2005 IEEE Ultrasonics Symposium, September 18, 2005 – September 21. 2005. Vol. 1. Rotterdam, Netherlands: Institute of Electrical and Electronics Engineers Inc, 2005. Pp. 329–332.

99. Schauer, A. & Roschy, M. R. F. SPUTTERED beta -TANTALUM AND B. C. C. TANTALUM FILMS. Thin Solid Films, 1972. Vol. 12, No. 2, pp. 313–317.

100. Berry, R.W., Hall, P.M. & Harris, M.T. Thin film technology. London, UK: Van Nostrand, 1968.

101. Nakao, S., Numata, M. & Ohmi, T. Thin and low-resistivity tantalum nitride diffusion barrier and giant-grain copper interconnects for advanced ULSI metallization. Japanese Journal Applied Physics, 1999. Vol. 38, pp. 2401–2405.

102. Oku, T., Kawakami, E., Uekubo, M., Takahiro, K., Yamaguchi, S. & Murakami, M. Diffusion barrier property of TaN between Si and Cu. Applied Surface Science, 1996. Vol. 99, No. 4, pp. 265–272.

103. Stavrev, M., Fischer, D., Wenzel, C., Drescher, K. & Mattern, N. Crystallographic and morphological characterization of reactively sputtered Ta, Ta-N and Ta-N-O thin films. Thin Solid Films, 1997. Vol. 307, No. 1–2, pp. 79–88.

104. Nie, H.B., Xu, S.Y., Wang, S.J., You, L.P., Yang, Z., Ong, C.K., Li, J. & Liew, T.Y.F. Structural and electrical properties of tantalum nitride thin films fabricated by using reactive radio-frequency magnetron sputtering. Applied Physics A: Materials Science and Processing, 2001 Vol. 73, No. 2, pp. 229–236.

105. Ezhilvalavan, S. & Tseng, T.Y. Electrical properties of Ta_2O_5 thin films deposited on Cu. Thin Solid Films, 2000. Vol. 360, No. 1–2, pp. 268–273.

106. Ezhilvalavan, S. & Tseng, T. Electrical properties of Ta_2O_5 thin films deposited on Ta. Applied Physics Letters, 1999. Vol. 74, No. 17, pp. 2477–2479.

107. Chaneliere, C., Autran, J.L., Devine, R.A.B. & Balland, B. Tantalum pentoxide (Ta_2O_5) thin films for advanced dielectric applications. Materials Science and Engineering R: Reports, 1998. Vol. 22, No. 6, pp. 269–322.

Appendices of this publication are not included in the PDF version. Please order the printed version to get the complete publication (http://www.vtt.fi/publications/index.jsp).

Series title, number and report code of publication

VTT Publications 716
VTT-PUBS 716-

Author(s)
Tommi Riekkinen

Title

Fabrication and characterization of ferro- and piezoelectric multilayer devices for high frequency applications

Abstract

By means of thin film technology a reduction of size, cost, and power consumption of electronic circuits can be achieved. The required specifications are attained by proper design and combinations of innovative materials and manufacturing technologies. This thesis focuses on the development and fabrication of low-loss ceramic thin film devices for radio and microwave frequency applications. The materials, growth conditions, and physical properties of the films and device structures are discussed in detail. Moreover, special emphasis is placed on the integration of highly conductive low-loss electrode materials into parallel-plate structures.

The thin films were prepared by sequential magnetron sputtering from metallic and ceramic deposition targets. The devices under study include tunable ferro-electric barium strontium titanate and lead strontium titanate parallel-plate capacitors, and piezoelectric aluminum nitride thin film bulk acoustic wave resonators. Furthermore, tantalum pentoxide and tantalum nitride thin films were investigated for capacitor and resistor applications. As electrode material we used Au, Cu, Mo, and Pt. The use of highly conductive low-loss Cu electrodes was only possible after the development of a new layer transfer fabrication method for parallel-plate ceramic devices. This method, which was successfully used to fabricate tunable ferroelectric capacitors and AlN bulk acoustic wave resonators, allows for high-quality ceramic film growth on suitable substrate and seed layers and, most importantly, deposition of the bottom and top electrodes after high-temperature reactive sputtering of the ceramic material.

Optimization of the ceramic growth conditions and the integration of these func-tional materials into low-loss parallel-plate structures resulted in state-of-the-art device performance. Key achievements include, device quality factors of more than 100 up to GHz frequency in ferroelectric parallel-plate capacitors, the tai-loring of ferroelectric film properties using substrate bias during magnetron sputtering, and very efficient electro-acoustic coupling in Mo/AlN/Mo bulk acoustic wave resonators.

ISBN
978-951-38-7356-1 (soft back ed.)
978-951-38-7357-8 (URL: http://www.vtt.fi/publications/index.jsp)

Series title and ISSN
VTT Publications
1235-0621 (soft back ed.)
1455-0849 (URL: http://www.vtt.fi/publications/index.jsp)

Project number
35811

Date
October 2009

Language
English

Pages
90 p. + app. 38 p.

Name of project

Commissioned by

Keywords
Ferroelectric, Piezoelectric, $Ba_xSr_{1-x}TiO_3$, $Pb_xSr_{1-x}TiO_3$, AlN, Ta_2N, Ta_2O_5, Paralle-plate capacitor, Dielectric tuning, Dielectric loss, RF applications

Publisher
VTT Technical Research Centre of Finland
P.O.Box 1000, FI-02044 VTT, Finland
Phone internat. +358 20 722 4520
Fax +358 20 722 4374

Julkaisun sarja, numero ja raporttikoodi

VTT Publications 716
VTT-PUBS 716-

Tekijä(t)
Tommi Riekkinen

Nimeke

Ferro- ja pietsosähköisten monikerroskomponenttien valmistus ja karakterisointi suurtaajuussovelluksiin

Tiivistelmä

Väitöstutkimuksessa perehdyttiin ohutkalvotekniikalla toteutettavien suurtaajuuspiirien rakennemateriaaleihin, niiden valmistustekniikkaan ja karakterisointiin. Ohutkalvotekniikan avulla voidaan toteuttaa pieniä, halpoja ja vähän energiaa vaativia komponentteja eri piiriratkaisuihin. Tämä vaatii uusien innovatiivisten materiaalien ja valmistusteknologioiden kehittämistä ja soveltamista. Tutkimuksessa kehitettiin pienihäviöisiä ohutkalvokomponentteja radio- ja mikroaaltotaajuussovelluksiin. Lisäksi kaikissa valmistetuissa rakenteissa käytettiin mahdollisimman hyvin johtavaa ja vähähäviöistä elektrodimateriaalia kriittisten suurtaajuushäviöiden vähentämiseksi.

Ohutkalvot valmistettiin sputteroimalla metalli- tai keraamikohtiosta. Työssä sovellettiin ferrosähköisiä bariumstrontium- ja lyijystrontiumtitanaatteja säädettäviin tasokondensaattorirakenteisiin. Tutkimuksessa kehitettiin myös valmistusprosessi pietsosähköisille alumiininitridiresonaattoreille suurtaajuussuodattimien rakenneosiksi. Lisäksi perehdyttiin ohutkalvokondensaattoreissa käytettävään tantaalipentoksidiin sekä ohutkalvovastuksissa sovellettavaan tantaalinitridiin. Elektrodimateriaaleina kaikissa rakenteissa käytettiin kultaa, kuparia, molybdeeniä tai platinaa. Väitöskirjassa esitetään lisäksi tapa valmistaa pienihäviöisiä ohutkalvorakenteita soveltamalla ns. kerrossiirtotekniikkaa. Tämä mahdollistaa minkä tahansa elektrodimateriaalin integroinnin rakenteisiin.

Tässä työssä valmistetut korkealaatuiset ohutkalvokomponentit ovat sovellettavissa suurtaajuusalueelle, ja ne edustavat alan tämän hetken uusinta tekniikkaa. Päätuloksina voidaan pitää ferrosähköisten komponenttien hyvyyslukua 100 yli GHz:n taajuusalueella, ferrosähköisten ohutkalvojen ominaisuuksien räätälöintiä substraattibiaksen avulla sekä korkeaa kytkentäkerrointa pietsosähköisissä resonaattoreissa.

ISBN
978-951-38-7356-1 (nid.)
978-951-38-7357-8 (URL: http://www.vtt.fi/publications/index.jsp)

Avainnimeke ja ISSN	Projektinumero
VTT Publications 1235-0621 (nid.) 1455-0849 (URL: http://www.vtt.fi/publications/index.jsp)	35811

Julkaisuaika	Kieli	Sivuja
Lokakuu 2009	Englanti	90 s. + liitt. 38 s.

Projektin nimi	Toimeksiantaja(t)

Avainsanat	Julkaisija
Ferroelectric, Piezoelectric, $Ba_xSr_{1-x}TiO_3$, $Pb_xSr_{1-x}TiO_3$, AlN, Ta_2N, Ta_2O_5, Paralle-plate capacitor, Dielectric tuning, Dielectric loss, RF applications	VTT PL 1000, 02044 VTT Puh. 020 722 4520 Faksi 020 722 4374

VTT PUBLICATIONS

ISBN 978-951-38-7356-1 (soft back ed.)
ISSN 1235-0621 (soft back ed.)

ISBN 978-951-38-7357-8 (URL: http://www.vtt.fi/publications/index.jsp)
ISSN 1455-0849 (URL: http://www.vtt.fi/publications/index.jsp)